THESIS FOR THE DEGREE OF DOCTOR OF PHILOSOPHY

Wetting and drying of aerogel-based coating mortars in Swedish climates

Ali Naman Karim

Division of Building Technology

Department of Architecture and Civil Engineering

CHALMERS UNIVERSITY OF TECHNOLOGY

Gothenburg, Sweden 2023

Wetting and drying of aerogel-based coating mortars in Swedish climates

Ali Naman Karim
ISBN 978-91-7905-925-5

Ny serie nr 5391
ISSN 0346-718X
Doktorsavhandlingar vid Chalmers tekniska högskola

Department of Architecture and Civil Engineering
Division of Building Technology
Chalmers University of Technology
SE-412 96 Gothenburg
Sweden
Telephone + 46 (0)31-772 1000

Author e-mail: ali.karim@chalmers.se

Chalmers Reproservice
Gothenburg, Sweden 2023

Wetting and drying of aerogel-based coating mortars in Swedish climates

ALI NAMAN KARIM
Department of Architecture and Civil Engineering
Division of Building Technology, Building Physics Modelling
Chalmers University of Technology

Abstract

Aerogel-based coating mortars (ACMs) have emerged as energy-efficient wall finishes with thermal conductivities of 30–50 mW/(m·K). These coating mortars represent a promising alternative to traditional thermal insulation materials for retrofitting uninsulated building envelopes particularly in culturally significant structures. Although previously used in Central Europe, their moisture absorption under rainwater wetting, early-stage drying, and long-term hygrothermal performance in other climates remain inadequately explored. This gap in knowledge presents challenges in designing moisture-safe solutions and evaluating in-field thermal insulation performance in regions characterized by high moisture loads and limited drying potential.

Therefore, an investigation was conducted to increase knowledge of the moisture performance of coating systems with ACMs. This investigation combined field and laboratory-based measurements with numerical hygrothermal simulations to study their moisture absorption under diverse wetting scenarios and evaluate their drying performance. Furthermore, the impact of surface water-repellent properties and surface cracks was assessed. The laboratory studies employed a newly developed small-scale test setup designed to simulate runoff wetting caused by typical wind-driven rain intensities in Sweden. Moreover, two supplementary capillary suction experiments under zero (free suction) and elevated hydrostatic pressure (created by Karsten tube) were conducted to explore additional wetting scenarios. A 15-month field test in Gothenburg, Sweden, combined with hygrothermal simulations were utilized to evaluate the early-stage drying and long-term hygrothermal performance of the coating system with ACM for four Swedish cities.

The laboratory measurements demonstrated minimal moisture absorption in the undamaged coating system with ACM, even during prolonged 24-h runoff wetting. As expected, applying water-repellent paint (s_d = 0.01 m) to the exterior of the coating system effectively reduced the water absorption while maintaining the drying capacity. Conversely, coating systems with a 1 ± 0.5 mm wide surface crack had 3–5 times amplified water intrusion due to hydrostatic pressure from the created water film on the surface. This could increase the risk of local moisture accumulation. Capillary suction tests of the ACM revealed a substantial increase in water absorption after repeated wetting exposure. Meanwhile, the same tests on the complete coating system showed a consistently stable water absorption. Field measurements indicated that the built-in moisture in the ACM dried out within six months. Hygrothermal simulations for four Swedish cities revealed an early-stage drying period ranging from 134 to 336 days based on the climate and time of application. Over time, the ACM exhibited no hygroscopic moisture accumulation; however, walls highly exposed to wind-driven rain could experience elevated relative humidity within the ACM, thereby resulting in an average increase in thermal conductivity of up to 9%. The findings show that the examined coating system with ACM presents a moisture-safe solution for retrofitting external homogenous concrete and masonry structures, preventing moisture accumulation from rainwater wetting. However, considering the information regarding the anticipated early-stage drying time and the moderate elevation in thermal conductivity is crucial when evaluating the in-field hygrothermal performance of the coating system.

Keywords: Aerogel, coating mortar, render, wetting, drying, wind-driven rain, runoff, retrofitting

Uppfuktning och uttorkning av aerogelbaserad puts i svenska klimatförhållanden

ALI NAMAN KARIM
Institutionen för Arkitektur och samhällsbyggnadsteknik
Avdelningen för Byggnadsteknologi, Byggnadsfysikalisk modellering
Chalmers tekniska högskola

Sammanfattning

Aerogelbaserad puts är del av energieffektiva invändiga och utvändiga putssystem med en värmeledningsförmåga på 30–50 mW/(m·K). De utgör ett lovande alternativ till konventionella isoleringsmaterial för renovering av oisolerade klimatskal särskilt i kulturhistoriskt värdefulla byggnader. Trots att de tidigare använts i Centraleuropa är deras fuktabsorption vid regnvattenbelastningar, uttorkning av initiala byggfukten samt långtidsuttorkning i andra klimat otillräckligt utforskade. Denna kunskapsbrist innebär utmaningar för att utforma fuktsäkra lösningar och utvärdera deras termiskt isolerande egenskaper i fält i regioner som kännetecknas av höga fuktbelastningar och begränsade uttorknings möjligheter.

För att öka förståelsen för fuktprestandan hos putssystem med aerogelbaserad puts genomfördes en undersökning som integrerade laboratorie- och fältmätningar, samt numeriska hygrotermiska simuleringar. Syftet var att studera putssystemens fuktupptagning under olika uppfuktningsscenarier och utvärdera deras uttorkningsprestanda. Dessutom utvärderades effekten av ytbehandlingens vattenavvisande egenskaper och ytsprickor. Laboratoriestudierna använde en nyutvecklad småskalig uppställning som var utformad för att simulera vattenavrinning på ytan orsakad av typiska slagregnsintensiteter i Sverige. Dessutom genomfördes två kompletterande kapillärsugningsexperiment under noll (fri sugning) och förhöjt hydrostatiskt tryck (skapat med hjälp av Karstenrör) för att utforska ytterligare uppfuktningsscenarier. Ett 15-månaders fältförsök i Göteborg, kombinerat med hygrotermiska simuleringar, användes för att utvärdera initial uttorkning och långsiktig hygrotermisk prestanda hos putsen i fyra svenska städer.

Laboratoriemätningarna visade minimal fuktupptagning i det oskadade putssystemet med aerogelbaserad puts, även under långvarig 24-timmars vattenavrinning på ytan. Som väntat minskade applicering av vattenavvisande färg (s_d = 0.01 m) på utsidan av putssystemet effektivt vattenupptagningen utan att kompromissa med dess uttorkningskapacitet. Å andra sidan hade putssystem med en 1 ± 0,5 mm bred ytspricka 3–5 gånger förstärkt vatteninträngning på grund av hydrostatiskt tryck från vattenfilmen på ytan, vilket ökar risken för lokal fuktackumulering. Kapillärsugningstesterna på den aerogelbaserade putsen visade en signifikant ökning av vattenupptaget efter upprepade uppfuktningsomgångar. Trots detta visade samma tester på de kompletta putssystemen med aerogelbaserad puts en mer stabil prestanda. Fältmätningarna indikerade att den inbyggda fukten i putsen torkade ut inom sex månader. Hygrotermiska simuleringar som utfördes i fyra svenska städer indikerade att uttorkningstiden av den initiala byggfukten varierade från 134 till 336 dagar, beroende på klimat och tidpunkt för applicering. På lång sikt uppvisade putssystemet ingen fuktackumulering. För väggar som är utsatta för kraftigt slagregn kan dock den förhöjda relativa fuktigheten i den aerogelbaserade putsen leda till en genomsnittlig ökning av värmeledningsförmågan med upp till 9%. Resultaten visar att det undersökta putssystemet utgör en fuktsäker lösning för renovering av utvändiga betong- och murverkskonstruktioner som effektivt hindrar fuktackumulering från regnvatten. Det är dock viktigt att beakta den förväntade torktiden i tidigt skede och ökningen av putsens värmeledningsförmåga vid utvärderingen av dess prestanda i fält.

Nyckelord: Aerogel, puts, uppfuktning, vattenavrinning, slagregn, uttorkning, renovering

List of Publications

This PhD thesis is based mainly on the work presented in the following publications:

Paper I Karim AN, Johansson P, Sasic Kalagasidis A. *Knowledge gaps regarding the hygrothermal and long-term performance of aerogel-based coating mortars*. Constructions and Building Materials 2022;314:125602. doi.org/10.1016/J.CONBUILDMAT.2021.125602

Paper II Karim AN, Johansson P, Sasic Kalagasidis A. *Increasing Water Absorptivity of an Aerogel-Based Coating Mortar in Subsequent Wetting and Drying*. Gels 2022, Vol 8, Page 764 2022;8:764. doi.org/10.3390/GELS8120764

Paper III Karim AN, Sasic Kalagasidis A, Johansson P. *Moisture absorption of an aerogel-based coating system under different wetting scenarios*. Submitted, 2023.

Paper IV Karim AN, Sasic Kalagasidis A, Johansson P. *Drying of aerogel-based coating mortars in Swedish climates: Field tests and simulations*. Submitted, 2023.

Authorship contribution statement: Paper I-IV

Ali Naman Karim: Methodology, Conceptualization, Validation, Visualization, Writing- original draft, review & editing, Formal analysis, Investigation, Literature review.

Additional Publications

Other publications that are related to the content of the thesis are listed below.

Conference articles:

a. Karim AN, Sasic Kalagasidis A, Johansson P. *Experimental study on the capillary water absorptivity of an aerogel-based coating mortar under subsequent drying and wetting cycles.* Proceedings of the 13th Nordic Symposium on Building Physics, Aalborg, Denmark, June 2023.

b. Karim AN, Johansson P, Sasic Kalagasidis A. *Duration of Early Stage Drying of Aerogel-based Renders: Field Tests and Simulations in Four Swedish Cities*. Proceedings of the 15th International Conference on Thermal Performance of the Exterior Envelope of Whole Buildings, Clearwater Beach, Florida, USA, December 2022.

c. Karim AN, Hagentoft C-E. *Determination of the Effective Thermal Conductivity of Aerogel-based Coating Mortars Using Numerical Simulations- Random Packing*. Proceedings of the 5th International Conference on Building Energy and Environment, Montreal, Canada, July 2022.

d. Hagentoft C-E, Karim AN. *Mathematical Expressions for Prediction of the Effective Thermal Conductivity of Perfectly Packed Two-phase Mixtures*. Proceedings of the 5th International Conference on Building Energy and Environment, Montreal, Canada, July 2022.

e. Karim AN, Adl-Zarrabi B, Johansson P, Sasic Kalagasidis A. *Determination of the anisotropic thermal conductivity of an aerogel-based plaster- using transient plane source method.* Proceedings of the 8th International Buildings Physics Conference 2021 (IBPC 2021), Copenhagen, Denmark, August 2021.

f. Karim AN, Johansson P, Sasic Kalagasidis A. *Super insulation plasters in renovation of buildings in Sweden: energy efficiency and possibilities with new building materials*. Proceedings of the World Sustainable Built Environment Conference (WSBE 2020), Beyond 2020, Gothenburg, Sweden, November 2020.

g. Karim AN, Johansson P, Sasic Kalagasidis A. *Long-term Performance of Silica Aerogel and Aerogel Based Composites: A Literature Review Highlighting Pathways for Further Studies*. Proceedings of the 14th International Vacuum Insulation Symposium (IVIS2019), Kyoto, Japan, September 2019.

Popular Science articles:

1. Karim AN, Johansson P, Sasic Kalagasidis A. *Superisolerande puts ett steg närmare verklighet i Sverige – erfarenheter från fältförsök.* Bygg och teknik, nr 2, p. 446–48, 2022 (In Swedish).
2. Karim AN, Johansson P, Sasic Kalagasidis A. *Aerogelbaserad puts- Superisolering för framtiden*. Husbyggaren, *nr 6, p. 88–11*, 2020 (In Swedish).

Acknowledgment

First, I would like to extend my sincere gratitude to my supervisors, Pär Johansson and Angela Sasic Kalagasidis, for their consistent support and invaluable feedback throughout my journey as a Ph.D. candidate. Their mentorship has played a pivotal role in shaping me into a more accomplished researcher, fostering the growth of my critical, creative, and independent thinking. I wish to express my gratefulness to Tang Luping for his dedicated role as my examiner and his consistent keen interest in my work. I am also deeply thankful to Bijan Adl-Zarrabi, Carl-Eric Hagentoft, and Paula Wahlgren for their valuable support and guidance during my time at Chalmers, both before and during my pursuit of Ph.D. My gratitude extends to my colleagues of the Division of Building Technology and the Building Physics Modelling research group. A special acknowledgment is owed to Fredrik Domhagen, who has been an invaluable friend, colleague, and roommate at Chalmers. I would also like to thank Sebastian Almfeldt and Anders Karlsson for their support in the laboratory. I am grateful to Samuel Brunner at Empa for his organization and facilitation of the study visit to Switzerland at the outset, and his ongoing interest in the research project is deeply appreciated.

Additionally, I would like to convey my thanks to the members of the reference group who contributed to this project. Your dedication and insightful contributions have substantially aided my work. A big thanks to Heck Wall-system in Germany and ROCKWOOL in Sweden for their collaboration and support in providing test materials. I am also grateful to Mölndala Fastighets AB for their valuable contribution in conducting the field test. The research was funded by the Swedish Energy Agency (46822-1 & P2022-00872). The financial support is gratefully acknowledged.

Finally, I want to express my heartfelt appreciation to my family and friends for their enormous support throughout this journey. Your encouragement has been a driving force behind my accomplishments.

Ali Naman Karim

Gothenburg, October 2023

Contents

Abstract ..... **I**
Sammanfattning ..... **II**
List of Publications ..... **III**
Acknowledgment ..... **V**
Contents ..... **VII**
1 Introduction **1**
1.1 Aim and objectives 2
1.2 Limitations 3
1.3 Overall research methodology 3
1.4 Thesis outline 5
2 Basics of and earlier investigations on ACMs **7**
2.1 Application process of ACM systems 9
2.2 Field studies in Europe 10
3 Wetting and drying in the laboratory **11**
3.1 Capillary wetting of ACM 11
3.1.1 Results 12
3.2 Wetting and drying of ACM systems 13
3.2.1 Runoff wetting 14
3.2.2 Complementary studies 17
3.2.3 Results 19
4 Drying of built-in moisture in ACM systems **23**
4.1 Field measurements 23
4.1.1 Results: Field measurements 25
4.2 Hygrothermal simulations 25
4.2.1 Early-stage drying of ACM 26
4.2.2 Hygrothermal performance of ACM in the field 27
4.2.3 Results: hygrothermal simulations 28
5 General discussions and reflections **29**
6 Practical recommendations for the application of ACMs in Sweden **33**
7 Conclusions **35**
8 Recommendations for future research **37**
References **39**

List of symbols

A_{cap}	Capillary water absorption coefficient (kg/(m^2 · min$^{0.5}$))
ACM	Aerogel-based coating mortar
ACM system	Coating system with aerogel-based coating mortar
AFR	Adhering fraction of rain (-)
ASHRAE	American Society of Heating, Refrigerating and Air-Conditioning Engineers
c_p	Specific heat capacity (J/(kg·K))
CV	Coefficient of variance (%)
P	Porosity (%)
RH	Relative humidity (%)
SD	Standard deviation
s_d-value	Diffusion-equivalent air layer thickness (m)
T	Temperature (°C)
TDS	Technical Data Sheet
U-value	Thermal transmittance (W/(m^2·K))
w	Moisture content (kg/m^3)
WDR	Wind-driven rain
WUFI	Wärme Und Feuchte Instationär

Greek symbols

μ	Water vapor permeability coefficient (-)
λ	Thermal conductivity (W/(m·K))
ρ	Density (kg/m^3)
σ_{ad}	Adhesive strength (N/mm^2)
σ_c	Compressive strength (N/mm^2)
σ_t	Tensile strength (N/mm^2)

Part I

Summary

1 Introduction

Over the past half-century, building regulations in Sweden have undergone multiple revisions, progressively tightening the energy performance requirements. There is currently a high demand for retrofitting and improving energy efficiency in residential buildings, multifamily houses, schools, and other premises [1,2]. According to the results of the BETSI project [3], a national investigation on the technical status of Swedish buildings in 2011, approximately 66% of all existing buildings exhibited various forms of damage and required light or deep retrofitting. Climate-related moisture damages and water leakages from installations included approximately 45% of the identified damages [1].

In this context, aerogel-based coating mortars (ACMs) have emerged as a promising class of multifunctional and energy-efficient materials for building energy retrofitting [4]. They were initially developed in Switzerland and introduced to the European market in 2012 [5]. ACMs are suitable for both internal (plaster) and external (render) applications, similar to conventional coating mortars. Commercial ACMs have a declared thermal conductivity of 30–50 mW/(m·K) [4], which falls within the range of conventional thermal insulation materials, such as mineral wool and expanded polystyrene. Meanwhile, ACMs exhibit a thermal conductivity that is over ten times lower than that of conventional coating mortars. Owing to their thermal insulation properties, ACMs can replace both the conventional coating mortar and additional insulation layers when retrofitting, e.g., concrete and brick masonry walls. As further elaborated in Section 2.1, ACMs are typically applied as part of a multilayer coating system (ACM system), accompanied by a few additional layers of conventional mortars, primarily to compensate for their lower mechanical strength.

Since 2012, the extensive use of ACMs has been reported in several Central European countries, including Germany and Switzerland [4]. However, ACMs have gained a little attention in Scandinavian countries, such as Sweden. The potential for ACM application in retrofitting existing buildings in Sweden is significant. Approximately 27% of multifamily buildings in Sweden, equivalent to around $(41 \pm 27)\cdot 10^6$ m^2 of façade area, feature conventional coating mortars [3]. It has been estimated that if only 10% of the coated façades of multifamily houses in Sweden are deemed suitable for ACM retrofitting, a minimum energy savings of 74 ± 48 GWh per year can be achieved [6]. In addition to the energy-saving potential of ACMs, they can enable a reduction in wall thickness, thereby increasing inhabitable space.

Moreover, ACMs present a unique solution for retrofitting culturally significant buildings, which often entails complex challenges. These include ensuring compatibility between new and existing materials, preserving character-defining elements, addressing moisture-related damage, and complying with building regulations regarding permissible envelope thickness [7]. In Sweden, only 41% of multifamily houses are deemed suitable for retrofitting their external walls with additional layers of traditional insulation materials [3]. In some of these cases, using ACM can potentially meet both the requirements of historical preservation and improve the energy performance of culturally significant structures.

The introduction of new technical solutions or materials, such as ACM, adapted from other regions in Central Europe, necessitates comprehensive evaluations and testing regarding the prevailing climate conditions, building techniques, and operations. This is crucial for avoiding costly serial failures of new solutions [8–10]. This significance is particularly evident in regions characterized by high moisture loads on buildings and limited drying potential, as shown by the south and west regions of Sweden with their subpolar oceanic climate [11]. This humid temperate climate subtype (Cfb) is characterized by elevated humidity levels and frequent rainfall throughout the year. Given the higher likelihood of moisture-related damages in these climates, moisture-safe design practices are adopted here more commonly than from other regions, including many parts of Central Europe where ACMs were originally developed and are commonly utilized. Notably, Sweden witnessed a relatively recent serial failure with the implementation of an imported external thermal insulation composite system (ETICS) [12]. This coating system was employed on a large scale in Swedish buildings in the early 2000s without adequate investigations into its suitability for the local climate and building techniques. Most cases involving ETICS resulted in severe moisture damage and substantial financial burdens. These failures in Sweden were primarily attributed to the lack of moisture-safe performance to withstand water leakage from precipitation and the vast availability of organic materials in wooden-based constructions. To ensure safe and reliable solutions with ACMs, conducting careful risk assessment analyses before their implementation in Sweden is essential.

As further elaborated in Chapter 2, extensive research has been conducted over the past decade on the energy-saving and thermal performance of ACMs. This research encompasses Central Europe and other countries, such as Italy, France, Portugal, and Canada. However, there remains a knowledge gap in understanding the moisture performance of ACMs, particularly regarding moisture absorption and drying performance under various rainwater wetting scenarios, including wind-driven rain (WDR). Furthermore, limited and scattered findings are available on the drying performance of ACMs in the field, which do not fully represent the prevailing Swedish climate. In addition, there exists a lack of data concerning the moisture performance of damaged coating systems, as previous research has primarily focused on intact and undamaged systems. This gap may be attributed to the relatively recent introduction of ACMs in the building industry and the lesser prevalence of moisture risk assessment analyses in the aforementioned regions. This lack of knowledge regarding the moisture performance of ACMs poses a barrier to developing moisture-safe design practices. Moreover, given the influence of moisture on the thermal performance of ACMs, this knowledge gap complicates the prediction of their thermal insulation performance in the field.

1.1 Aim and objectives

This study primarily aims to advance the understanding and knowledge regarding the moisture performance of ACMs, specifically within the context of Swedish climates and their external application on massive concrete and masonry walls. The research investigates the moisture absorption of ACM systems under various rainwater wetting scenarios and their early-stage drying and hygrothermal performance in field applications. The influence of surface water-repellent properties and surface defects on moisture absorption and drying performance is also examined.

More specifically, the work is structured around the following questions:

1. Which moisture absorption properties does the ACM system exhibit under (rainwater) wetting?

2. How do moisture absorption properties differ between a damaged ACM system with a surface defect and an undamaged ACM system?

3. How does the drying process of the ACM system progress in Swedish climates?

4. What is the expected thermal insulation performance of the ACM system when applied in Swedish climates and under rainwater exposure?

1.2 Limitations

This thesis focuses on investigating the hygrothermal performance of ACMs, limited to moisture absorption at wetting and subsequent drying. Only one commercial ACM product and its associated coating system were examined; no other ACM products or mortar combinations within the coating system were subjected to evaluation. In addition, the analyses are primarily focused on the climate conditions in Sweden. The investigations specifically concentrate on the external application of ACMs on massive masonry walls because these structures constitute the most culturally significant buildings in Sweden that undergo retrofitting.

1.3 Overall research methodology

The following section provides an account of the developmental and research history of the Ph.D. journey, along with a rationale for selecting research methods. Figure 1 illustrates the methodology framework. The research commenced with a comprehensive literature review to systematically survey the available data on ACMs and identify knowledge gaps in this field. Simultaneously, study visits were made to a commercial ACM manufacturing facility and several buildings retrofitted with ACMs in Switzerland. These visits focused on acquiring insights into the material characteristics of ACMs and gathering practical information regarding the application process of ACM systems on façades. Moreover, standardized laboratory tests were conducted to investigate the hygrothermal properties of ACMs that lacked sufficient data in the literature. The outcomes of these investigations were presented in the Licentiate thesis [8] and **Paper I**. Considering the identified knowledge gaps in the literature, the research questions outlined in Section 1.1 were formulated. Subsequently, a research methodology was developed that combined laboratory-based measurements and pilot studies, field measurements, and numerical hygrothermal simulations.

The capillary water absorption of the ACM as a standalone material subjected to consecutive rounds of capillary wetting and drying was examined in **Paper II**. This laboratory-based study was initiated in response to unexpected observations made during the initial standard measurements conducted at the outset of the research project. While investigating the repeatability of the standard capillary water suction tests, a repetitive increase was observed in the water absorption of the ACM samples. This observation has not been previously reported or elucidated in the literature.

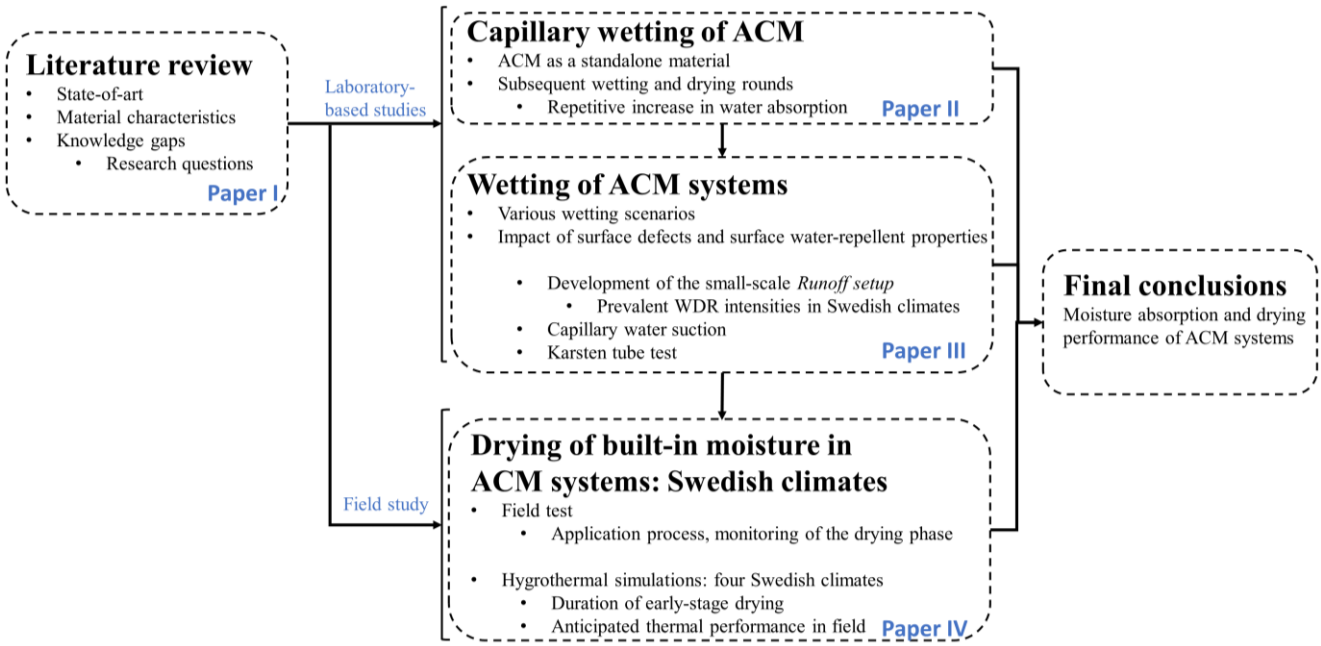

Figure 1. Research methodology framework.

The research presented in **Paper III** involved a laboratory pilot study to measure the moisture absorption of an ACM system when exposed to wetting based on the prevalent WDR intensities in Swedish climates. Furthermore, the study aimed to assess the influence of surface defects and water-repellent coating on the moisture absorption and drying performance of the coating system. Standardized test methods exist for estimating the watertightness of wall assemblies to WDR. These tests employ an absolute pass/fail criterion to determine the watertightness of large-scale test walls under specified pressure differences. Notably, the test conditions used in these methods, including applied water intensity and pressure differences, are often considered extreme and are more applicable to high-rise buildings. Moreover, as ACM systems serve a multifunctional role as both external coating mortar and primary thermal insulation components in walls, an absolute pass/fail criterion for their watertightness may not adequately evaluate their moisture and thermal performance. Understanding the moisture distribution within the ACM system during wetting and subsequent drying phases is crucial in determining the extent of moisture penetration into the ACM. The amount of moisture that reaches the ACM directly affects its thermal insulation properties, which is a critical factor in practical applications.

As discussed in **Paper III**, a small-scale setup was developed to test the ACM system under various surface conditions. The test method aimed to address three key criteria that distinguish it from the existing standard methods utilized to assess the watertightness of wall assemblies against WDR. First, the focus was on the capability to simulate low-intensity WDR loads representative of the prevalent WDR events in Swedish climates. Second, the tests were conducted on a small scale, offering increased efficiency and ease of testing compared to current methods that usually require large test walls. Third, monitoring systems were implemented to enable continuous and real-time tracking of total moisture absorption and moisture distribution within different depths of the ACM system during the wetting and drying phases.

Initially, attempts were made to replicate WDR using water spray nozzles following standardized testing methods. However, achieving the desired low water intensity proved challenging owing to limitations in using low-flow (dimming) nozzles. These nozzles produced relatively small water droplets and provided limited surface area coverage. Although increasing the targeted intensity or using

multiple nozzles were potential alternatives, they were deemed unfeasible for implementation in the setup due to deviations from representative WDR intensities in Sweden. Furthermore, the monitoring systems integrated into the setup required verification procedures as they had not been previously employed for testing ACM systems. Considering the challenges encountered and the potential uncertainty arising from unexpected measurement results discussed in **Paper II** regarding water absorption analysis of the investigated ACM, the current wetting scenario in the setup was limited to water runoff.

To address this simplification, two complementary studies were included to investigate alternative wetting scenarios with higher pressure applied to the coating system. The first study employed the capillary suction test, which subjected the coating system to greater overpressure than that in the runoff setup. A comparative analysis of the capillary water absorption performance between the ACM as a standalone material and the ACM system was facilitated by adopting similar wetting and drying conditions as in **Paper II**. The second study utilized the Karsten tube method, which employed hydrostatic pressure generated by a water column to simulate water absorption under high pressures. Specifically, these pressures corresponded to wind velocities of up to 43 m/s, exceeding the pressures exerted in the other two studies. This approach provided further insight into the moisture absorption of the coating system under more extreme conditions.

In the study presented in **Paper IV**, a field test was conducted in Sweden to monitor the early-stage drying of the ACM system under real outdoor climate conditions. This field test also gathered insights from the application process of the coating system. To complement the field test, numerical hygrothermal simulations were utilized to predict the duration of the ACM's early-stage drying phase in four Swedish cities. In addition, the study investigated the expected thermal insulation performance of the ACM when subjected to rainwater absorption in the field.

1.4 Thesis outline

The thesis comprises eight chapters summarizing the research presented in the appended papers **I–IV**. Following an introductory Chapter 1, Chapter 2 presents the state-of-the-art of ACMs, drawing from the literature review presented in **Paper I**. It focuses on elucidating the material properties of ACMs and offering a detailed account of the practical application processes involved in ACM systems. Furthermore, it provides an overview of previous field tests conducted in Europe to provide a broader context for the research. Chapter 3 encompasses the laboratory measurements and summarizes the work presented in **Papers II** and **III**. It highlights the findings obtained from investigating the capillary water absorption performance of ACMs and assessing the moisture absorption and drying characteristics of ACM systems under various wetting scenarios. Chapter 4 centers on the field measurements and hygrothermal simulations presented in **Paper IV**, which investigates the early-stage drying and hygrothermal performance of the ACM system based on the climates of four Swedish cities. Chapter 5 includes general discussions on the conducted research and the author's reflections on the various research studies conducted during the Ph.D. journey. In Chapter 6, practical recommendations for applying ACMs in Sweden are compiled. Finally, Chapters 7 and 8 consolidate the findings into general conclusions and provide recommendations for future research in this field, respectively.

2 Basics of and earlier investigations on ACMs

The development of ACMs commenced in the early 2010s. The first publication by Stahl et al. [5] in 2012 marked the beginning of research on the material properties, hygrothermal performance, and practical application of ACMs [13–15]. Concurrently, research groups in Germany, Italy, France, Austria, Portugal, the United Kingdom, Canada, China, Norway, and Sweden have also contributed to the field, focusing on the development, characterization, and evaluation of ACMs. ACMs have primarily been utilized in buildings located in Central European countries. By 2017, ACMs covered approximately 30,000 m^2 of façade area in Switzerland alone [13] and around 100,000 m^2 of façade area in Europe by 2019 [16].

Similar to conventional coating mortars, the material composition of ACMs comprises binders, aggregates, and additives [8]. Table 1 presents a list of commercial ACMs and their key components. ACMs typically employ lime- and cement-based binders and additives, such as air-entraining and hydrophobic agents. The primary distinction between ACMs and conventional coating mortars lies in the aggregates. In ACMs, sand is replaced by aerogel granules (Figure 2). Aerogels are nanostructured superinsulation materials with high porosity (over 95%) and thermal conductivities ranging from 10 to 20 mW/(m·K). The synthesis process of aerogels involves multiple steps [17,18], preserving a three-dimensional network with significant porosity. Surface modifications are also applied to achieve hydrophobic properties and protect the solid network against humid environments. Aerogels possess attributes, such as low density (typically 100 kg/m^3), fragility and low mechanical strength, and a high surface area (600–1,000 m^2/g) [4]. Among the aerogel variants, mesoporous silica (SiO_2) aerogels are predominantly utilized in building applications.

Table 1. Commercial ACM products and their main components.

Products	Country	Internal/External application	Ingredients
Product 1	Switzerland	Both	Hydraulic lime NHL 5, calcium hydroxide, white cement, aerogel granules, light mineral aggregate, water retaining agent, air-entraining agent, hydrophobic agent
Product 2	Switzerland	Both	Hydrated lime, white cement, aerogel granules, light mineral aggregate, organic components, and additives to improve the processing properties
Product 3	Switzerland	Both	Hydraulic lime, hydrated white lime, white cement, aerogel granules, light aggregate, water retaining agents, air-entraining agents, water-repellent agents
Product 4	Germany	External	White cement, hydrated lime, aerogel granules, mineral lightweight aggregates
Product 5	Germany	Internal	White cement (chromate-free), hydrated lime, aerogel granules, mineral lightweight aggregates
Product 6	Germany	Both	Calcium hydroxide, cement, silica granules, perlite
Product 7	Germany	Both	Calcium hydroxide, cement, silica granulate, perlite
Product 8	Germany	Both	Calcium hydroxide, cement, silica granulate, perlite
Product 9	Germany	Both	Calcium hydroxide, cement, silica granulate, perlite
Product 10	Germany	Both	White cement, natural hydraulic lime NHL 5, Poraver (an expanded glass granule produced by the company of Poraver), aerogel, air-entraining agent, cellulose ether, dispersion powder based on vinyl acetate and ethylene, starch Ether

Table 2 presents the range of declared material properties for commercial ACMs. Due to the significant proportion of aerogel granules, typically exceeding 50 vol%, ACMs exhibit characteristics, such as low density, mechanical strength, and thermal conductivity. The declared thermal conductivities of commercial ACMs range from 26 to 52 mW/(m·K), while their densities range from 180 to 290 kg/m^3. The literature review in **Paper I** revealed a lack of readily available material properties for commercially available ACMs, including temperature- and moisture-dependent thermal conductivity, heat capacity, flexural and adhesive strength, and moisture sorption isotherms with a hysteresis effect. Furthermore, the moisture absorption properties of ACMs when subjected to various types of wetting have not yet been fully investigated. Limited research has been conducted on the long-term durability of ACMs, primarily focusing on accelerated aging tests. Consequently, drawing definitive conclusions about the stability and long-term performance of ACMs is challenging. Finally, previous research has not extensively explored the hygrothermal and mechanical compatibility of ACMs with adjacent materials in ACM systems. The lack of adequate data on the material properties necessary to understand moisture absorption under wetting and the drying performance of the ACMs inspired the research studies conducted and presented in this thesis.

Table 2. Range of material properties for commercial ACMs.

Property	Minimum	Maximum	Average	Number of products reporting data on the property
ρ (kg/m^3)	180	290	215	10 out of 10
P (%)	45	90	67.5	2 out of 10
c_p (J/kg·K)	-	-	-	0 out of 10
λ (mW/(m·K))	26	52	35.3	10 out of 10
σ_c (N/mm^2)	0.4	0.8	0.49	8 out of 10
σ_t (N/mm^2)	-	-	-	0 out of 10
σ_{ad} (N/mm^2)	0.08	0.08	0.08	1 out of 10
A_{cap} (kg/(m^2·s$^{0.5}$))	W_c2 (<0.2)	W_c0: no specified value	W_c1 (<0.4)	8 out of 10
μ-value (−)	4	6	5.05	9 out of 10

Similar to conventional coating mortars, the fresh mortar of ACMs is prepared by blending the dry ACM mixture with water. Subsequently, the prepared fresh mortar is applied manually or with spray machines, as illustrated in Figure 2. As discussed in Chapter 1, ACMs are commonly utilized in an ACM system, which is elaborated upon in Section 2.1.

Figure 2. a) Aerogel granules. b) Dry mixture of ACM. c) Preparation of fresh mortar by blending the ACM with water. d) Application with spray machine. e) Application by hand.

2.1 Application process of ACM systems

A schematic representation of a typical ACM system is depicted in Figure 3. This coating system comprises multiple layers, each applied individually and allowed to dry before adding the subsequent layer [4]. The coating process begins with an initial undercoat, which improves adhesion and regulates water absorption by the substrate. Subsequently, the ACM layer, with a thickness typically ranging from 10–50 mm, is applied. A primer is added, followed by an outer coating mortar imparting mechanical strength. In some cases, a glass-fiber reinforcement mesh may be incorporated. After drying, a second layer of outer coating mortar is applied. The coating system may be supplemented with mineral-based (silicon), vapor-open, and water-repellent paint to achieve the desired surface properties and appearance. The addition of these layers typically increases the total thickness of the coating system by approximately 10 mm. For instance, if a 40 mm ACM layer is to be applied, the resulting ACM system will have a thickness of around 50 mm. Table 3 provides the approximate layer thicknesses and required drying time before applying the subsequent layer in the coating system. Photographs illustrating the various steps in applying the ACM system are presented in Figure 4, captured during the field test discussed in **Paper IV**. As stated in the ACMs' Technical Data Sheet (TDS), protecting the coating system from adverse weather conditions is imperative. This includes extreme temperatures (both high and low: below +5°C), precipitation, solar radiation exposure, and wind. To ensure optimal conditions during the application phase, which typically spans a minimum of around 50 days, weather protection measures, such as the utilization of weather protection (Figure 4a), along with the potential use of a heating element, can be implemented.

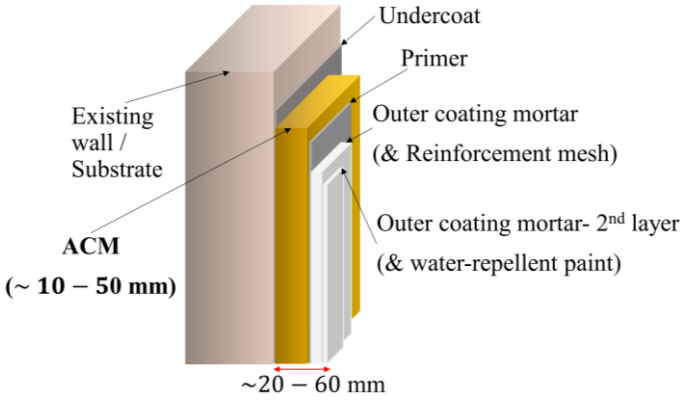

Figure 3. Schematic representation (not to scale) of the ACM system, illustrating the sequential application of individual layers, including an initial undercoat, the ACM layer, a primer, outer coating mortar, and optional incorporation of reinforcement mesh and paint. The presence of additional layers beyond the ACM layer induced an approximate increase of 10 mm in the overall thickness of the coating system.

Table 3. Thickness and minimum drying time of each layer in the ACM system of typical values.

Layers in the ACM system	Thickness (mm)	Minimum drying time (day)
Undercoat	-	1
ACM	40	28
Primer	-	1
Outer coating mortar (and mesh)	5	5
Outer coating mortar (second layer)	4	14
Water-repellent paint (three steps)		
Primer	-	1
paint	-	1
Paint (second layer)	-	1
Total	50	52

Figure 4. Photographs (**Paper IV**) illustrating the step-by-step application process of the ACM system. The photograph in (a) demonstrates the use of weather protection to mitigate weather-related stresses during the application phase. The process includes preparation (b), removal of the existing coating mortar, and cleaning of the substrate, followed by the successive application of an undercoat (c), ACM (d), the first layer of outer mortar with reinforcement mesh (e), the second layer of outer mortar, and finally, the water-repellent paint. The final appearance of the coating system after the removal of the weather protection is depicted in (f).

2.2 Field studies in Europe

Paper I presents a comprehensive review of previously conducted field studies on ACMs from 2012 to 2021. The analysis identified 12 full-scale studies conducted on ACMs, encompassing varying-scale renovation projects. Tables 15 and Table 16 in **Paper I** provide a compilation of key details extracted from the studies reported in the literature. The application of ACMs ranged from individual façade elements to entire building surfaces. The studies were conducted in Switzerland, France, Austria, Germany, Italy, and Norway, focusing on buildings with uninsulated envelopes. Brick or concrete façades were predominant in 11 out of 12 cases. The thickness of ACMs applied was 5 cm or less in 7 out of 12 studies, with the majority (10 out of 12) applying the ACMs externally. The primary emphasis of these studies was on ACM's thermal performance. Eight studies explicitly reported improved thermal performance with the addition of 1.5–6 cm of ACM, which reduced thermal transmittance (U-value) by 27%–70% for the investigated walls. Four studies demonstrated a U-value reduction of over 50%. Furthermore, three studies indicated a decrease in moisture damage risk and enhanced thermal comfort with the incorporation of ACMs. Except for one report of minor visible cracks, no significant cases of damage associated with ACM application were identified.

3 Wetting and drying in the laboratory

This chapter presents the experimental studies conducted in the laboratory to investigate the moisture absorption and drying performance of ACM systems under three wetting scenarios. The findings summarized in this chapter are derived from **Papers II** and **III**.

3.1 Capillary wetting of ACM

This section summarizes the laboratory measurements presented in **Paper II**, focusing on the capillary water absorption of an ACM. As indicated in Chapter 2, previous studies investigating the capillary water absorption of ACMs are limited to a few studies [19–25]. These studies reported the capillary water absorption coefficient, A_{cap} (kg/[$m^2 \cdot min^{0.5}$]), of noncommercial ACMs based on a single round of measurement following the EN ISO 1015-18 standard [26]. The reported A_{cap} values ranged from 0.48 to 2.8 kg/($m^2 \cdot min^{0.5}$), calculated as one-tenth of the mass increase during the 10–90-min capillary water absorption period. Meanwhile, the stated requirement for the A_{cap} of thermal insulation mortars, including ACMs, is set to be less than 0.4 kg/($m^2 \cdot min^{0.5}$) [27]. Apart from these studies, insufficient information exists regarding the long-term capillary water absorption of ACMs, which could include exposure to multiple rounds of wetting and drying when applied in the field.

Therefore, the capillary water absorptivity of a commercial ACM exposed to subsequent wetting and drying rounds was measured. Figure 5 provides an overview of the preparation and testing procedures implemented. The measurements involved four sets of ACM samples, each comprising three identical cubic samples. The samples were subjected to three rounds of wetting and drying, and the resulting water mass gain (kg/m^3) due to capillary water absorption was measured. Table 4 presents the declared material properties of the studied ACM [28].

Table 4. Declared material properties of the studied ACM [28].

Material property	Unit	Declared value
Bulk Density (ρ)	(kg/m^3)	180
Thermal conductivity (λ)	mW/(m·K)	40
Water vapor permeability coefficient (μ-value)	-	≤ 5
Water absorption coefficient (A_{cap})	kg/($m^2 \cdot min^{0.5}$)	W_c2 (<0.2)
Compressive strength (σ_c)	N/mm^2	CS I (<0.5)

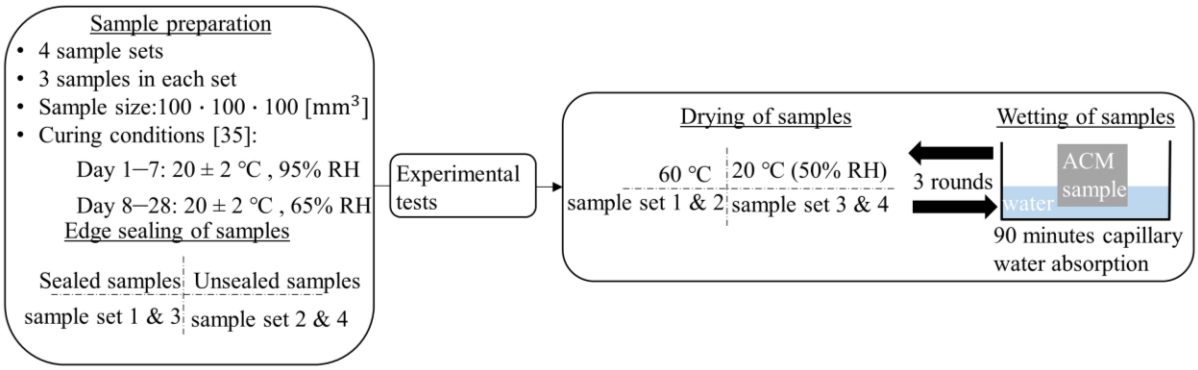

Figure 5. Schematic representation of the experimental procedure employed to assess the capillary water absorption of ACM samples undergoing three consecutive rounds of wetting and drying. Four sets of samples, comprising 12 samples, were prepared and subjected to different drying conditions.

In the experimental procedure depicted in Figure 5, each testing round commenced with the drying of ACM samples. Sample sets 1 and 2 were subjected to drying in a ventilated oven at an elevated temperature of 60°C ± 5°C [26]. Conversely, Sample sets 3 and 4 underwent drying at room temperature of 20°C ± 0.5°C with a relative humidity (RH) of 50% ± 2%. This choice aimed to evaluate the influence of the drying conditions on the water absorptivity measurements of the ACM samples. The drying process concluded when each sample maintained a constant mass, following the recommendations provided in [26]. While all sides, except one, of the samples in Sample sets 1 and 3 were sealed using epoxy glue, the samples in Sample sets 2 and 4 remained unsealed. This variation in sealing conditions among the sample sets was implemented to investigate the impact of the recommended side sealing method outlined in the standard [26] on the measurement outcomes. For clarity and coherence with the study presented in Section 3.2.2, which employed the same experimental conditions on the complete ACM system, this section primarily centers on the results obtained from Sample set 3. The reader is referred to the appended **Paper II** for comprehensive findings on Sample sets 1, 2, and 4 as well as detailed discussions regarding the influence of the selected sealing and drying conditions.

For each measurement round, each ACM sample was placed in an enclosed container and maintained in continuous contact with water for 90 min. The water level in the containers was maintained at a minimum of 5–10 mm [26], and the water mass gain of each ACM sample was measured at specific time intervals of 10, 20, 45, and 90 min.

3.1.1 Results

Figure 6 illustrates the measured water mass gain (kg/m^2) over a period of 90 min for Sample set 3, containing sealed samples that were dried under room conditions (20°C, 50% RH). The corresponding standard deviation (SD) is also provided for each measurement point. The presented results represent the average values obtained from all three samples within Sample set 3. Comprehensive results of Sample sets 1, 2, and 4 are available in **Paper II**.

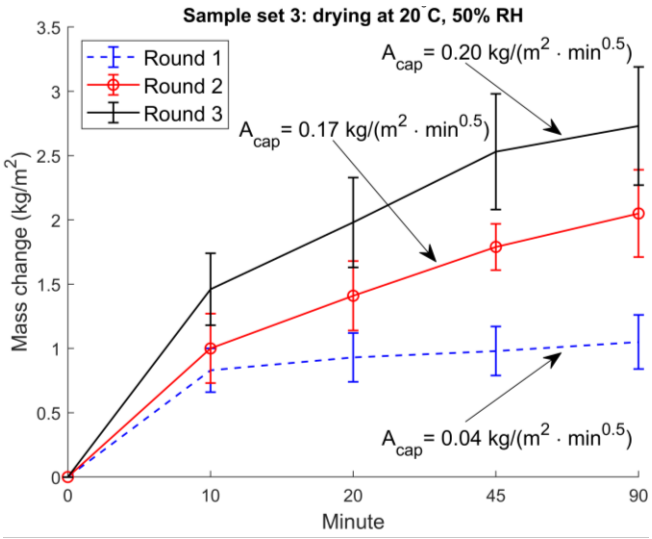

Figure 6. Measured water mass change of sealed ACM samples in Sample set 3 during 90 min of capillary water absorption and drying at room conditions (20°C, 50% RH).

The results indicate increased mass gain due to capillary water absorption after each round of wetting and drying. The average mass gain during the first round was 1.05 kg/m^2, while in the third round, it reached 2.73 kg/m^2, showing a 2.6-fold increase compared to the initial round. The corresponding A_{cap} after the third round was calculated to be 0.20 kg/(m^2·min$^{0.5}$), which is five times higher than the A_{cap} calculated after the first round (0.04 kg/[m^2·min$^{0.5}$]). Notably, the increase rate between the second and third rounds was reduced, with the average mass gain in the third round being approximately 1.95 times higher than that in the second round.

Similar outcomes were observed for the remaining three sample sets, where alternative sealing and drying conditions were tested. The calculated A_{cap} values during the initial round ranged from 0.04 to 0.06 kg/(m^2·min$^{0.5}$), whereas after three rounds of wetting and drying, these values increased to 0.17–0.27 kg/(m^2·min$^{0.5}$), indicating an over fivefold rise compared to the first round. While drying and sealing conditions may influence the results, they cannot solely account for the substantial increase in water absorptivity. The coefficient of variance (CV) for the measurements, representing the relationship between the calculated SD and the mean value, varied between 7% and 22% for each sample set. This variability suggests remarkable differences among the measurement results in some sets, potentially stemming from sample heterogeneity, uncertainties associated with manual weighing, or scale accuracy. However, these measurement uncertainties do not explain the observed over fivefold increase in water absorptivity after the third cycle. Possible explanations for this phenomenon involve the low mechanical strength of the ACM causing microcracking, reduced hydrophobicity, and inhomogeneous moisture distribution and pore structure of the ACM after each drying cycle. These structural alterations may introduce new moisture flow paths, contributing to higher capillary water absorption. Further experimental investigations are necessary to validate these hypotheses and ascertain whether this observed phenomenon applies to all ACMs.

3.2 Wetting and drying of ACM systems

Section 3.2 provides a concise overview of the laboratory measurements conducted in **Paper III**, focusing on the moisture absorption and drying performance of the ACM system with different surface conditions when subjected to three different wetting scenarios.

Figure 7 presents a schematic of the conducted studies. In Section 3.2.1, the primary investigation involves runoff wetting of the ACM system in the developed runoff setup. Section 3.2.2 encompasses two complementary studies: the capillary water suction test and the Karsten tube test. In the first study, capillary water absorption tests are conducted under free suction conditions. In the second study by the Karsten tube method, the water absorption process will simulate overpressures of up to 1,100 Pa, achieved through the hydrostatic pressure of a 100 mm height water column (10 ml).

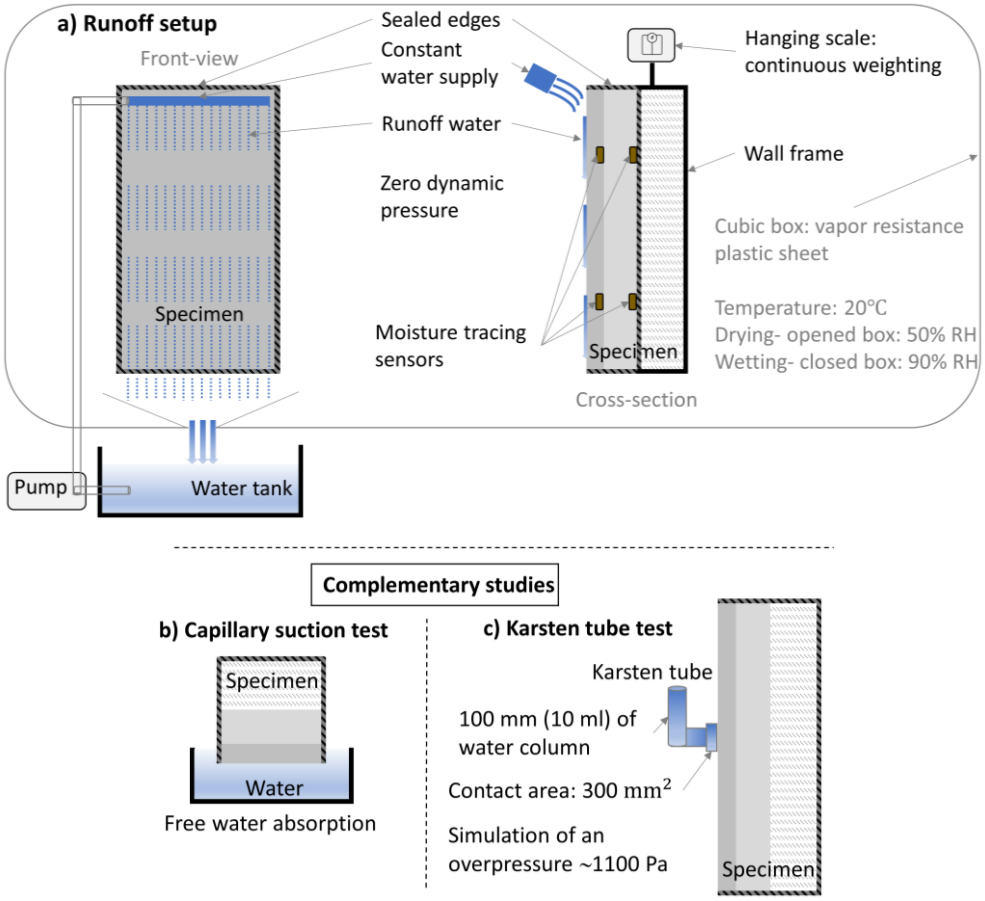

Figure 7. Schematic representation of the experimental studies conducted. a) Main study utilizing the runoff setup. Specimens exposed to water runoff without applied surface pressure. b) Capillary water absorption test involving water soaking from one side of the specimens. c) Karsten tube measurements to assess water absorptivity under high pressures of up to 1,100 Pa, corresponding to pressure on a windward façade due to a wind velocity of 43 m/s.

3.2.1 Runoff wetting

The runoff setup in its current configuration was developed to simulate rainwater runoff on the external surface of the specimens (ACM system). Schematic illustration (Figure 7a) and corresponding photographs (Figure 8) showcase the constructed setup. The setup comprised a cubic box with internal dimensions of 1.4 × 1.5 × 0.75 m³ (height × width × depth). Vapor-resistant plastic sheets (μ-value: $3 \cdot 10^5$) were applied to the exterior of the cube, featuring a detachable front screen. The setup installation occurred within a controlled environment (20°C ± 1°C, 50% ± 2% RH). During the wetting phase, the box remained closed to maintain high humidity (90% ± 5% RH), emulating the moisture conditions experienced during rainfall and minimizing evaporation from the wet surface of the specimens. Conversely, the front of the box was opened during the drying phase to facilitate drying toward 50% RH. The specimen was mounted within a rectangular wall frame, possessing an inner surface area of 6.1 × 4.1 m² (height × width) and a weight of 4.4 kg. The frame was suspended from a hanging scale

(Figure 8c) to monitor changes in mass throughout the measurement process. The employed hanging scale (OIML C2.S) had a maximum capacity of 50 kg and a declared sensitivity and mechanical accuracy of 2 mV/V and ± 0.025 kg, respectively. During the experiments, an average of 1000 data points was collected and logged at one-minute intervals. The weighing system underwent calibration for a measurement range of 0–25 kg, with a maximum error of 1%. Within the mass change range relevant to the conducted measurements, the weighing system error was below 0.01 kg. Besides, two moisture tracing sensors were positioned behind the outer coating mortar (approximately 9 mm from the external surface) and two behind the ACM (approximately 49 mm from the external surface) and situated in the vertical center of the upper and lower halves of the specimens. Before the experiment, the sensors were calibrated in a controlled chamber at a constant temperature of 20°C and RH levels of 50%, 70%, 85%, 95%, and a wet condition (100% RH). Further information regarding the setup and monitoring systems can be found in **Paper III**.

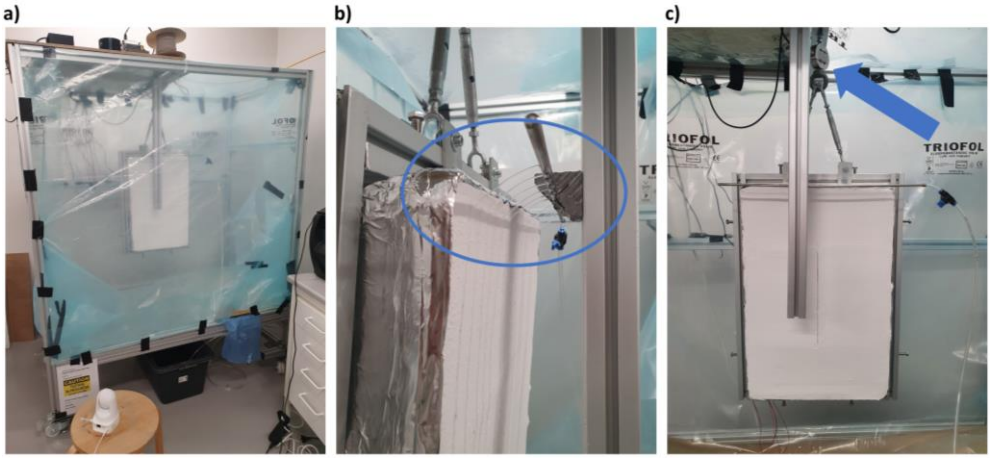

Figure 8. a) Wetting phase with closed box (90% ± 5% RH) in a climate-controlled room (20°C, 50% RH). b) Water distributor pipe positioned in front of the specimen (indicated by a blue oval) with continuous water flow through 15 circular openings (1 mm inner diameter). c) Specimen suspended from a hanging scale (blue arrow) for continuous weighing throughout wetting and drying.

A water supply system was developed to simulate rainwater runoff on the exterior of the specimens. The water flow rate was determined based on a case study presented in Appendix A of **Paper III**, which analyzed the most frequent WDR intensities in Swedish climates. The maximum estimated water runoff on the windward façade of a three-story building with a height of 15 m during a one-hour WDR event was below 22 L/h. To ensure conservative testing conditions, a water flow rate of 30 L/h (equivalent to approximately 2 L/[m^2·min] considering the specimen surface area) was selected. Water was uniformly distributed on the specimen surface through a fixed-position stainless-steel pipe located 70 mm in front of the specimen (Figure 8b). The pipe featured 15 circular openings with a 1 mm inner diameter and a center-to-center distance of 25 mm. Water streams emitted from these openings simulated rainwater runoff, striking the upper portion of the specimen. The water runoff was re-circulated back to the water tank through an outlet hole at the bottom of the setup.

Specimens for the ACM system of 0.6 m in height and 0.4 mm in width were prepared based on the procedures outlined in Section 2.1 and Figure 3. An aerated concrete block served as the substrate. Before applying the ACM system, all surfaces of the substrate and later the sides of the finalized test specimen were sealed to ensure that the experiment was unaffected by the substrate and to restrict moisture exchange with the surroundings solely to the exterior surface. Table 5 presents the material properties of the key layers of the ACM system. Four specimens were prepared, each characterized by varying surface conditions. To ensure consistency and clarity in the study, these four specimen types of

the ACM system will be designated and subsequently referred to as Façade I–IV, as depicted in Figure 9a. Façades I and II were undamaged, as shown in Figure 3. Façade II was externally coated with a mineral-based (silicon), vapor-open, and water-repellent paint recommended by the producer for use of the ACM. However, the outermost layer of the reference case, Façade I, remained unpainted. Two damaged specimens were included to investigate the influence of surface cracks on the performance of the coating system. Façades III and IV exhibited horizontal and vertical surface cracks, respectively. These cracks were created by inserting a 0.3 mm-thick metal sheet into both layers of the outer coating mortar during the fresh stage (Figure 9b-c). Due to the fragility of the ACM, any mechanical impact on the hardened coating mortar could lead to breakage or inconsistent cracks. Ultimately, the cracks reached a depth of approximately 9 mm, protruding through the entire outer coating layer to the front side of the ACM. The average width of the cracks at the final hardened stage was 1 ± 0.5 mm. Centered on the surface, the cracks spanned a length of 300 mm.

Table 5. Material properties of the key layers in the coating system.

	ACM		Outer coating mortar	Water-repellent paint
Thickness (mm)	40		9	-
Vapor permeability, μ-value (–)	3[a]		10[d]	s_d-value 0.01 m [d]
Water absorption coefficient, A_{cap} ($kg/(m^2 \cdot min^{0.5})$)	0.04[b]		0.08[b]	0.01–0.06 [d]
Thermal conductivity, λ (mW/(m·K))	RH (%)	λ[c]	λ_{dry}: 900 [d]	-
	0	40		
	80	45		
	90	50		
	100	400		

Measured in the laboratory: [a]- 1015-19 [29], [b]– EN 1015-18 [26], [c]– ISO 22007-2 [30]. [d]– Declared value [28].

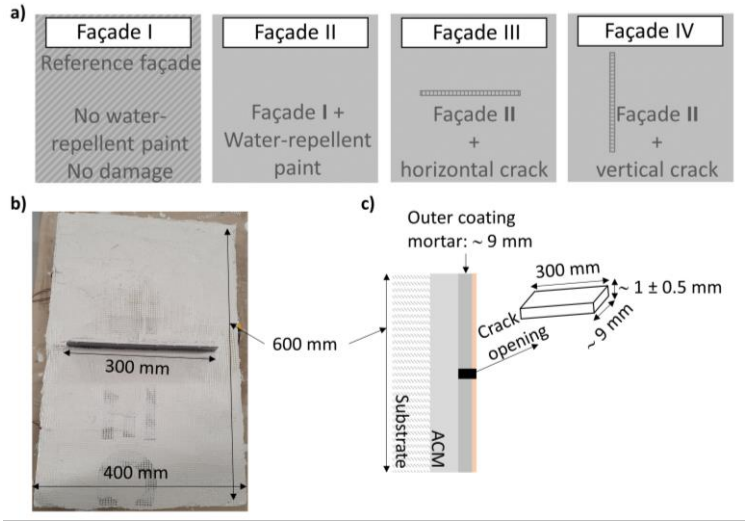

Figure 9. a) Four distinct types of specimens/façades employed in the measurements. b-c) Creation of surface cracks in Façade III and IV. A metal sheet was inserted through both layers of the fresh outer mortar to generate a vertical (Figure 8c) or horizontal crack. b) Photograph depicting the metal sheet penetrating the first layer of outer mortar and mesh for a horizontal crack (Façade III). c) Schematic representation (not to scale) illustrating the dimensions of the final crack opening at the hardened stage, with an average width of 1 ± 0.5 mm, a depth of approximately 9 mm, and a length of 300 mm.

Table 6 presents the experimental parameters for the measurements conducted in the runoff setup. In each test (Façade I–IV), two identical specimens (specimens 1 and 2) were considered to measure the repeatability of the results. Six rounds of wetting and drying were performed for each façade. The wetting phase, designed to simulate an extended period of rainfall, lasted for 24 h. To accommodate the time-intensive nature of the subsequent drying process, it was divided into two distinct phases. Initially, the first 144 h (6 days) of drying occurred within the runoff setup, with the specimen suspended from the scale and the plastic chamber opened on one side. Subsequently, the sample was relocated to another area within the climate room and allowed to dry naturally until it reached its initial mass. On average, the time elapsed between two successive wetting events for the same specimen exceeded 60 days.

Table 6. Measurement scheme for the study using the runoff setup.

Runoff setup	Façade I	Façade II	Façade III	Façade IV
Surface quality	No water-repellent paint, no damage	Water-repellent paint, no damage	Water-repellent paint, one horizontal crack	Water-repellent paint, one vertical crack
Number of specimens	2	2	2	2
Number of wetting and drying rounds	3	3	3	3
Duration of wetting phase	24 h	24 h	24 h	24 h
Duration of drying phase in the setup [a]	144 h	144 h	144 h	144 h

[a]: The remaining time until complete drying back to the initial state was completed outside the setup in the same climate room (20°C, 50% RH).

3.2.2 Complementary studies

In the first complementary study, the capillary water absorption of the ACM system was evaluated following the methodology described in the previous study (Section 3.1: sealed ACM Sample set 3, drying at 20°C, 50% RH) and standard EN ISO 1015-18 [26]. Specimens of the coating system, with a surface area of 100 × 100 mm², were prepared, and the substrate (plywood) and the sides of the finalized samples were sealed. For each façade type (I–III), nine measurements (3 specimens × 3 wetting rounds) were performed. In this study, only one damaged façade (denoted as Façade III) was included as the orientation of the crack was irrelevant when the specimens were vertically soaked in water. The 30-mm long cracks were centered on the surface and had a width of 1 ± 0.5 mm and a depth of 9 mm. Figure 10a-b illustrates the measurement setup and the prepared specimens. The mass gain (kg/m²) of the samples was recorded at specific time intervals, including 10, 20, 45, 60, and 90 min, and after 24 h of wetting. Table 7 summarizes the key aspects related to the measurements.

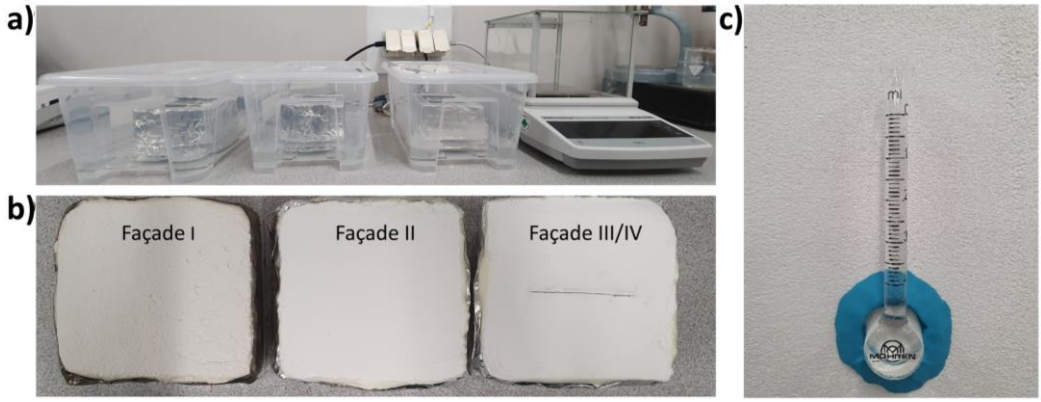

Figure 10. a) Measurement setup for capillary water suction tests. b) Specimens with a surface area of 100 × 100 mm² were immersed from one side in 5–10 mm of water while all other sides were sealed. c) Karsten tube attached to a façade. A constant water pressure generated by a 10 ml water column aimed to simulate pressures up to 1,100 Pa on the surface equivalent to a wind velocity of 43 m/s.

Table 7. Measurement scheme for the capillary suction tests.

Capillary water suction	Façade I	Façade II	Façade III/IV[a]
Surface quality	No water-repellent paint, no damage	Water-repellent paint, no damage	Water-repellent paint, one crack
Number of specimens	3	3	3
Number of wetting and drying rounds	3	3	3
Duration of wetting phase	24 h	24 h	24 h

[a]: In these measurements, the orientation of the crack (vertical or horizontal) was irrelevant. Thus, only one type of damaged specimen (Façade III/IV) was considered.

The second complementary study involved the application of the Karsten tube method, which currently lacks established standards but relies on recommendations from literature, such as [31–33]. A dome with a diameter of 30 mm and a cylindrical tube with a volume of 10 ml (equivalent to a 100 mm head of water) constituted the Karsten tube apparatus. It was attached to the façades, as depicted in Figure 10c. By exerting hydrostatic water pressure, the Karsten tube method emulated an overpressure of 1,100 Pa corresponding to a wind velocity of 43 m/s. The absorbed water was manually measured by monitoring the reduction in water volume within the tube at 1, 5, 10, 15, 30, 60, and 90 min of wetting. Any decrease of 1 ml in volume was replenished to ensure consistent pressure on the surface. Given the limited contact surface area of the dome, the wetting phase was constrained to a duration of 90 min. Prolonged wetting would lead to water absorption by the surrounding material due to capillary forces, causing the wetting area to expand into an undefined shape and extend beyond the applied pressure. Table 8 presents the details of the measurements conducted. The Karsten tube test was exclusively conducted on undamaged Façades I and II, as applying this test on a cracked surface was deemed inappropriate due to immediate absorption through the crack opening.

Table 8. Measurement scheme for the Karsten tube tests.

Karsten tube method	Façade I	Façade II
Surface quality	No water-repellent paint, no damage	Water-repellent paint, no damage
Number of specimens	1	1
Number of wetting rounds	6	6
Duration of wetting phase	1.5 h	1.5 h

3.2.3 Results

This section presents the findings of the main study and the complementary studies described in Sections 3.21 and 3.2.2, respectively. A comprehensive analysis and discussion of the results can be found in **Paper III**.

Table 9 summarizes the total range of mass gain and loss (kg/m^2) for all specimens of Façades I–IV during the 24-hour wetting and the initial 144-hour drying phases in the runoff setup. The table also includes the maximum RH at lower positions in the test specimens (A_{down} and B_{down} in Figure 11) at the end of both the wetting and drying phases. For more detailed measurement results, the reader is referred to Figure 9–12 in **Paper III**. The reference Façade I and the one with water-repellent paint (Façade II) exhibited similar performance during the wetting and drying phases. However, during the initial 10 h of wetting, Façade II exhibited an average mass gain of up to 6% (0.04 kg/m^2) lower than that of Façade I. This difference could indicate a higher runoff rate for Façade II and a higher absorption rate for Façade I. Conversely, after 24 h of wetting, Façade II had a 9% (0.07 kg/m^2) higher average mass gain than Façade I, suggesting increased water runoff as the outermost layer of Façade I became saturated. In the initial 144 h of drying, approximately 85% (0.52 kg/m^2) of the absorbed moisture in both Façades I and II was removed. The average drying rate differed by around 2% between Façades I and II at the end of the 144-hour drying period.

Both the undamaged Façades I and II exhibited comparable RH trends with minor deviations. The average RH at positions A_{down} (and A_{up}), behind the outer mortar, reached a peak of around 96% during wetting and decreased to a minimum of 54% during the initial 144 h of drying. Behind the ACM, at positions B_{up} (and B_{down}), the highest average RH was recorded at 65% and 62% for Façades I and II, respectively, approximately 6 h and 4 h after the end of wetting. At position B_{down}, Façade I displayed a maximum RH of 59% after wetting, while Façade II reached a peak RH of 64% around 5 h after wetting. The increasing RH behind the ACM following the cessation of wetting indicates moisture redistribution within the ACM toward the interior (substrate). After 144 h of drying, the RH at positions B_{up} and B_{down} decreased to approximately 52% for both Façades I and II.

The response of Façades III and IV to identical runoff wetting exhibited scattered patterns featuring vertical and horizontal cracks, respectively. In three out of six measurement rounds, the mass gain of Façades III and IV (0.6–0.9 kg/m^2) resembled that of undamaged Façades I and II (0.6–0.7 kg/m^2), indicating minimal water penetration through the cracks. During the initial 144 h of drying, approximately 85%–95% of the absorbed moisture was eliminated. However, in the remaining three and four measurement rounds for damaged Façades III and IV, respectively, the mass gain (1.9–3.2 kg/m^2) exceeded that of undamaged Façades I and II by a factor of 3–5. Notably, sudden increases in the mass change rate were observed after 5–20 h of wetting during these rounds, and approximately 50%–65% of the absorbed moisture was dried out during the 144 h of drying.

Figure 11 provides insight into the highest RHs observed at lower positions in the damaged Façades III and IV compared to the measured RHs at lower positions in Façades I and II. Behind the outer mortar (A_{down}), the RH rapidly reached 95%–100% within the first hour of wetting for Façades III and IV. While the RH decreased at A_{up} during the drying process, the RH at A_{down} remained consistently high (above 95%) for the initial 120 h of drying. This observation suggests moisture redistribution from the upper sections to the lower sections of the specimens due to gravity. Similar trends were noticed for the RHs behind the ACM with the RH decreasing at B_{up} and increasing at B_{down} during the initial drying phase. The RHs behind the ACM increased to 85%–95% before gradually declining toward 50% of RH.

Table 9. Total mass change in all six measurement rounds (2 specimens × 3 rounds) and maximum RH registered in Façades I–IV during wetting and drying phases. More details can be found in Figures 9–12 in **Paper III**.

	Façade I	Façade II	Façade III	Façade IV
End of 24 hours of wetting				
Mass gain (kg/m^3)	0.6–0.7	0.7–0.8	0.6–3.2	0.7–2.9
$RH_{outer\ mortar} - A_{down}$ (%)	96	97	100	100
$RH_{ACM} - B_{down}$ (%)	64	71	70	70
End of 144 hours drying				
Mass loss (kg/m^3)	0.53–0.55	0.62–0.63	0.55–1.63	0.52–1.34
$RH_{outer\ mortar} - A_{down}$ (%)	59	57	88	82
$RH_{ACM} - B_{down}$ (%)	50	54	95	65

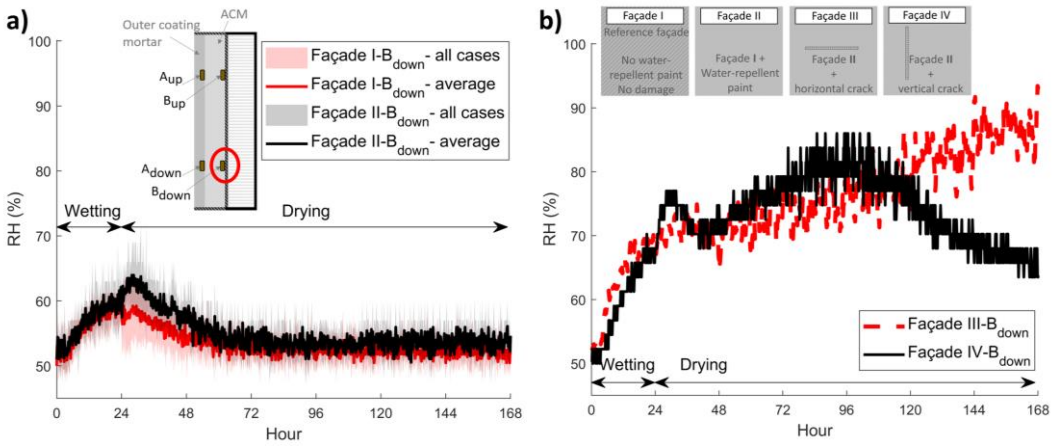

Figure 11. a) measured RH at the lower parts of Façades I and II in the runoff setup. The shaded graphs depict the total variability across all six measurement rounds (2 specimens × 3 rounds) for each Façades I and II. b) measured RH at the lower parts of Façades III and IV with the highest water abortion during wetting in the runoff setup.

Figure 12a presents the results of three rounds of capillary suction tests and the corresponding SD. Façade II demonstrated the lowest total water suction, while the damaged Façade III exhibited the highest mass gain at 90 and 1,440 min (24 h) of wetting. After 24 h, Façade II absorbed approximately 50% less water than Façade I, whereas Façade III absorbed approximately 13% more water than Façade I. Figure 12b presents the mass change for each round of measurement for Façade I. Related details for Façades II and III are available in **Paper III** (Figure 14). At 90 min of wetting, the mass change in the second and third rounds of measurements deviated by no more than 7% from the first round. After 24 h of wetting, the mass gain in the second and third rounds increased by up to 10% and 13% for Façades I and II, respectively. However, for Façade III, the mass gain in the second and third rounds decreased by up to 7%. The CV for the Façades I, II, and III measurements ranged from 10% to 23%, 7% to 25%, and 3% to 28%, respectively. In a previous study discussed in Section 3.1 (Figure 6), similar tests conducted on ACM samples revealed a 2.6-fold increase in water absorptivity after three rounds of 90-min capillary water suction tests, corresponding to five times higher A_{cap}. These findings indicate that while the ACM system showed a modest change of less than 7% after three rounds, it exhibited a more stable performance than ACM used as a standalone material.

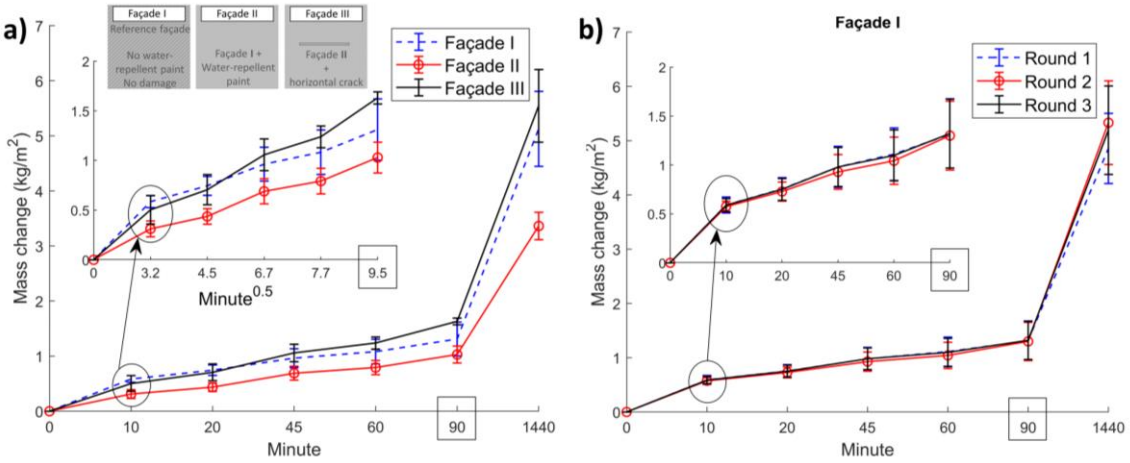

Figure 12. a) Average capillary water suction (kg/m^2) and SD for three rounds of measurements on Façades I, II, and III at 90 and 1,440 min (24 h). b) Capillary water suction (kg/m^2) for each measurement round for Façade I. The embedded plots represent the water suction during the first 90 min, using an x-axis scale of minute$^{0.5}$ (90 min → 9.5 min$^{0.5}$).

Figure 13 presents the results of the Karsten tube test conducted on Façades I and II. The findings reveal a consistently lower water absorption for Façade II than for Façade I. Notably, Façade II exhibited approximately 75% and 51% less water absorption than Façade I after 5 and 90 min of wetting, respectively. The former may pertain to the water absorption during a concise WDR event lasting only a few min. The CV for the measurements on Façade I ranged from 10% to 31%, while for Façade II, it ranged from 15% to 22%.

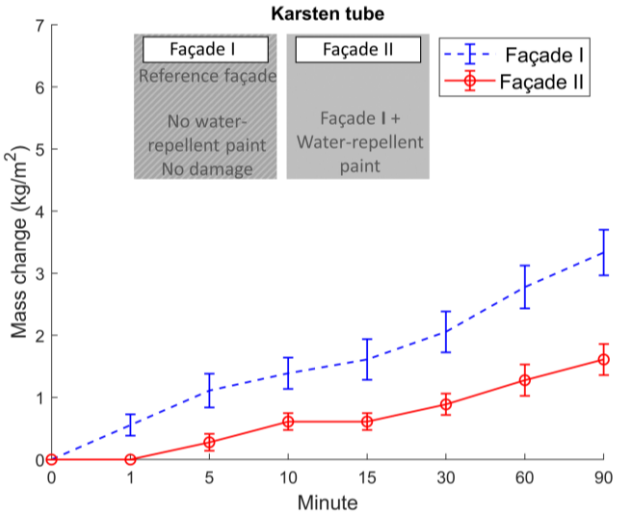

Figure 13. Water absorption results of the Karsten tube test for Façades I and II over 90 min.

Figure 14 presents a comparative analysis of maximum water absorption in Façades I–IV under three wetting scenarios: runoff, capillary suction, and Karsten tube. The analysis includes short-term (90 min) and long-term (24 h) wetting durations. The figure provides the absolute mass change (kg/m^2) and relative mass gain of Façades II, III, and IV relative to Façade I for each wetting scenario. Notably, there is a significant difference in crack length between the damaged façades used in the runoff setup (crack length: 300 mm, wall surface: 600 × 400 mm^2, ratio: 5/10 or 7.5/10) and those used in the capillary suction test (crack length: 30 mm, wall surface: 100 × 100 mm^2, ratio: 3/10).

Among the wetting scenarios considered, runoff wetting demonstrated the lowest water absorption for all façades. Façade III exhibited the highest mass gain during runoff wetting, with approximate values of 1.0 kg/m^2 at 90 min and 3.2 kg/m^2 at 24 h. In contrast, Façade I showed lower values of 0.4 kg/m^2 at 90 min and 0.6 kg/m^2 at 24 h. Compared to Façade I, Façade II with water-repellent paint displayed a reduction of approximately 15% in mass change during short-term wetting and an increase of 9% during long-term wetting. Among Façades III and IV, Façade III with a horizontal crack exhibited the highest maximum mass increase.

In the capillary suction test, Façade II exhibited the lowest mass increase, while the damaged Façade III displayed the highest mass increase at long-term wetting. The water absorption of Façade II was 28% lower at 90 min and 37% lower at 24 h than that of Façade I. Conversely, the water absorption of Façade III was 1% lower at 90 min and 11% higher at 24 h than that of Façade I. Façade II showed a 50% lower water absorption in the Karsten tube wetting than Façade I. As shown in Figure 13, Façade II exhibited negligible water absorption after one minute, while Façade I exhibited absorption of approximately 0.6 kg/m^2. This value is comparable to the average water absorption of Façade I during 24 h of runoff wetting. The mass increase of Façade I after 90 min of Karsten tube wetting was around 4.0 kg/m^2, whereas, for capillary suction and runoff wetting, it was approximately 1.7 and 0.35 kg/m^2, respectively. That is, wetting involving high-pressure differences over the façade (1,100 Pa, corresponding to a wind velocity of up to 43 m/s) resulted in 2–12 times greater water absorption than wetting with low/zero hydrostatic pressure.

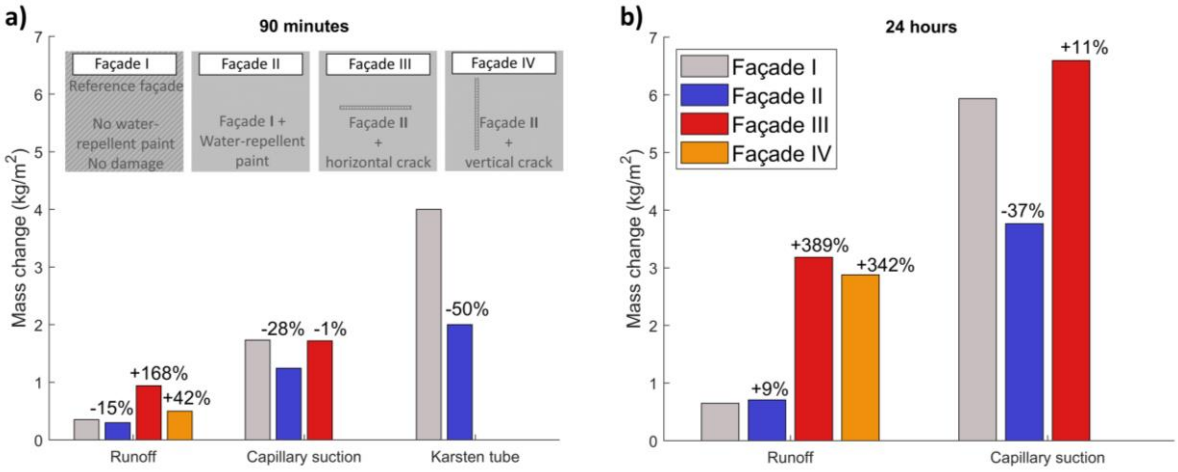

Figure 14. Comparative analysis of maximum water absorption among Façades I–IV under different wetting scenarios at short-term [90 min: (a)] and long-term [24 h: (b)] durations. The relative mass gain (($V_2 - V_1$)/ V_1) between Façades II, III, and IV (V_2) and Façade I (V_1) for each wetting scenario is indicated. Given the irrelevant crack orientation, the capillary suction test included only Façade III as the damaged wall. The Karsten tube tests were conducted exclusively using Façades I and II.

4 Drying of built-in moisture in ACM systems

This chapter summarizes the work presented in the appended **Paper IV**. The study encompassed a field measurement that spanned 15 months and focused on monitoring the early-stage drying of the ACM-system. Additionally, numerical hygrothermal simulations were used to evaluate the early-stage drying and hygrothermal performance of the ACM in four different cities across Sweden.

4.1 Field measurements

To evaluate the drying characteristics of the ACM system, a field test was conducted in Gothenburg, a city situated on the west coast of Sweden. The investigation focused on a limited section of the northeast façade of a rendered brick building dating back to 1921. A wall partition measuring approximately 3 m^2 was selected for the study, where it was coated with the ACM system, as detailed in Section 2.1. Additionally, another identical wall partition on the same façade underwent a comparative analysis as a reference test wall. This reference wall was covered with an undercoat and approximately 10 mm of conventional lime and cement-based coating mortar. Figure 15 shows the completed construction of the reference test wall and the wall coated with ACM. Both test walls were treated with the same water-repellent paint described in Section 3.2.1 and Table 5. The application procedure followed the guidelines outlined in Chapter 2.1(Figure 4 and Table 3).

The hygrothermal conditions in the test walls were monitored by placing temperature and RH sensors at different depths and heights, as illustrated in Figure 16. For the ACM-coated wall, sensors were positioned at three different depths: in the middle of the brick wall (P1), behind the ACM layer (P2), and behind the outer coating mortar (P3). In the case of the reference test wall, sensors were placed at two depths: in the middle of the brick wall ($P1_{ref}$) and behind the conventional coating mortar ($P2_{ref}$). At each position, three sensors were installed at different heights (up, middle, and down). The sensors utilized in this study were wood moisture sensors (Sahlén sensors). These sensors determine moisture content expressed as RH, utilizing the sorption isotherm of the wooden probe (birch) surrounding the sensor. To measure the outdoor conditions near the test walls, an additional sensor was placed outdoors, shielded from solar radiation.

The sensors had an accuracy of ±2.5% within the range of 10 to 90% RH and ±0.5°C at 25°C. Measurements were taken every 10 min, from which hourly and seven-day moving averages were calculated. Due to restrictions imposed by the tenants, it was not feasible to monitor the interior climate of the building. The monitoring period spanned January 1, 2022–March 31, 2023, covering 15 months.

During this period, the building was partially occupied and heated, although it was in substandard condition due to its imminent demolition. Consequently, the interior climate was expected to be primarily influenced by outdoor conditions rather than consistent heating.

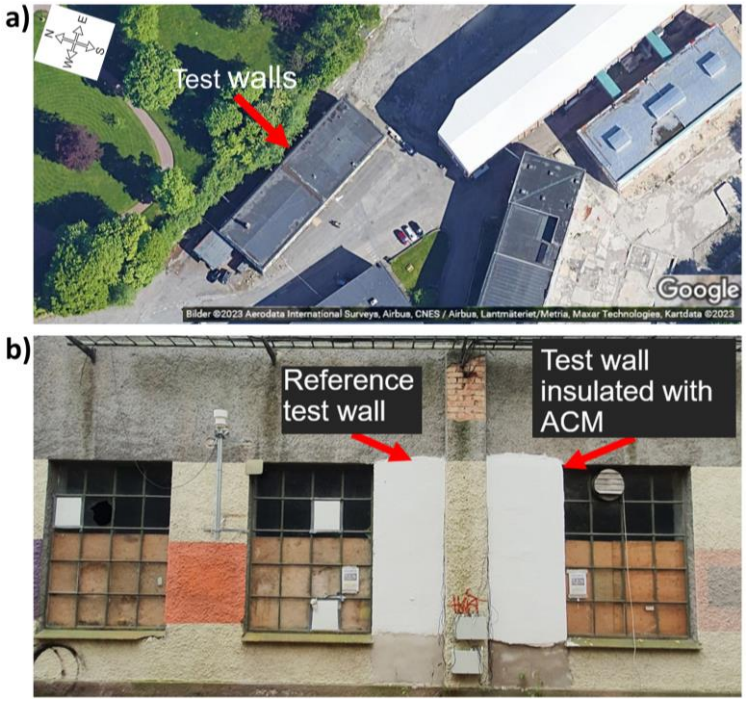

Figure 15. a) Overview depicting the location of the test building and the corresponding façade included in the field test (source: Google Maps). b) Photograph of the reference test wall and the test wall covered by the ACM system. The two test walls had a surface area of approximately 3 m^2 each and were located on the northeast façade of a brick building in Gothenburg, Sweden.

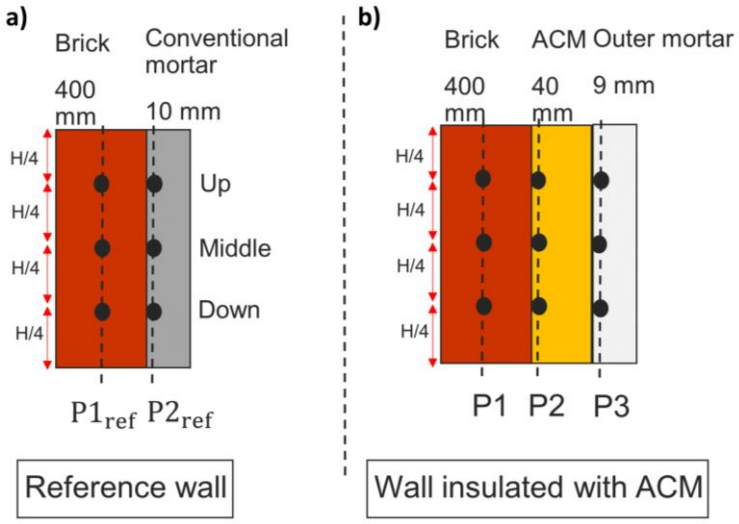

Figure 16. Schematic diagram showing the arrangement and labeling of sensors in the reference test wall (a) and the wall coated with ACM (b). Three sensors were evenly distributed at each position along the height (H) of the test walls: up, middle, and down. Both test walls were externally coated with white water-repellent paint. Images of the sensors at positions P2 and P3 can be seen in Figure 4c and Figure 4d, respectively.

4.1.1 Results: Field measurements

Figure 17 shows the seven-day moving average of the measured RHs for the wall insulated with the ACM system. Further measurement results can be found in **Paper IV**. The presented values represent the average RH from three sensors located at each position along the walls (up, middle, and down). The maximum variation in RH among the three sensors at any position ranged from 3% to 11%.

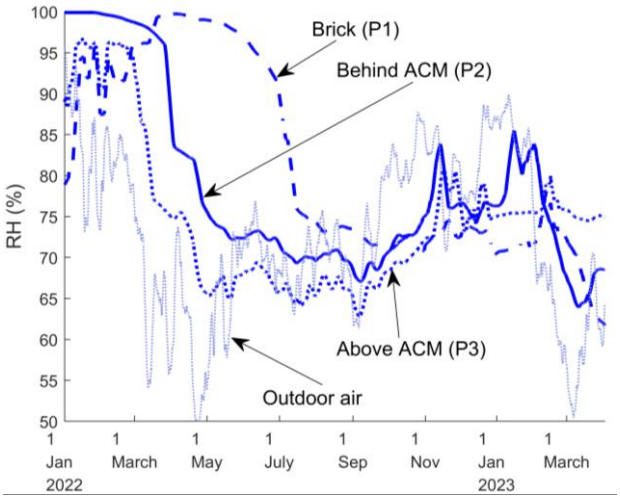

Figure 17. Seven-day moving average of RH measurements at different positions in the ACM-insulated wall. The values at each position represent the average of three sensors (top, middle, and bottom).

The measured RHs in the ACM-insulated wall indicated that the built-in moisture in the ACM system and the initially wet ACM dissipated within approximately six months. Throughout this period, moisture redistribution occurred from the saturated coating system to the underlying brick wall (from P2 and P3 to P1), resulting in elevated RH levels within the brick and decreased RH levels within the coating system. A similar drying trend and moisture redistribution were observed in the reference wall, albeit with a comparatively faster drying rate. The ACM system, with a thickness of approximately 50 mm, exhibited a longer drying time than the conventional coating mortar, which had a thickness of 10 mm. RH levels behind the outer mortar (P3) and the conventional mortar in the reference wall ($P2_{ref}$), with similar thicknesses of approximately 10 mm, displayed comparable performance. Once the built-in moisture of the ACM system dissipated, the RH levels in the ACM-insulated wall (P1–P3) closely tracked the RH fluctuations in outdoor air. No moisture accumulation was observed within the coating system during the initial 15-month monitoring period.

4.2 Hygrothermal simulations

One-dimensional (1D) and two-dimensional (2D) numerical hygrothermal simulations were utilized to investigate the early-stage drying and hygrothermal performance of the ACM system in the field. The simulations were conducted using the building physics software WUFI [34] version 3.4. The details of the simulation model and the verification study conducted are presented in **Paper IV**.

The thickness and material properties of the construction layers used in the simulations were derived from the test wall with ACM described in Section 4.1. A parametric study, presented in Appendix A of **Paper IV**, was conducted to determine two unknown parameters: the interior climate and the material properties of the existing brick wall. The brick type "brick masonry" from the WUFI database was selected based on its closest agreement with the filed measurements. The interior temperatures were assumed to be 5°C higher than the exterior air temperatures, accounting for the building's thermal

inertia and additional heating. No interior moisture supply was considered, and the interior RHs were calculated accordingly. To represent the water-repellent paint, additional vapor resistance with an s_d-value of 0.01 m [28] was applied to the exterior boundary surface.

4.2.1 Early-stage drying of ACM

The early-stage drying period was defined as the time necessary for the built-in moisture within the initially wet and saturated ACM to dry out. The drying process was considered complete when the maximum RH behind the ACM, at position P2 (Figure 16), reached 70%. The commencement of the early-stage drying was determined when the ACM system was constructed and the weather protection was removed, coinciding with January 1, 2022, in the field test. To ensure accuracy, complete drying was recognized only when the RH remained below 80% for a minimum of 30 consecutive days following the attainment of the 70% RH threshold. The drying criterion of 70% RH was chosen as a conservative threshold, considering the moisture-dependent thermal conductivity of the ACM (Table 5). In the simulations, four Swedish cities representing diverse geographical locations were selected: Gothenburg (west coast), Stockholm (east coast), Östersund (central), and Kiruna (north). The built-in weather data files from WUFI, containing typical values from 1995 to 2005, were employed. Table 10 provides an overview of the weather conditions in these four cities.

To explore the impact of different application times on the duration of the ACM's early-stage drying, four distinct application dates were examined for each of the four cities. The drying process was assumed to be initiated on January 1, March 1, June 1, and September 1. The initial moisture content in the ACM system was assumed to be completely wet and saturated (100% RH), while the brick wall was assumed to have an average RH of 80%. The orientation of the test wall was set to north, representing the orientation with the least drying potential across all four cities. A construction without any leakage and a fully water-repellent paint were assumed for the exterior, resulting in an adhering fraction of rain (AFR) of 0. In WUFI, AFR is a unitless parameter that determines the proportion of rainwater available for capillary water absorption on the façades. A value of 1 indicates full absorption availability, while 0 signifies no capillary absorption. For moderately exposed façades, a recommended AFR value of 0.7 [35] is used.

Table 10. Overview of the weather conditions in the four cities considered for hygrothermal simulations. Data were extracted from the weather data file in WUFI [34].

	Gothenburg	Stockholm	Östersund	Kiruna
Köppen–Geiger Climate Classification [11] [a]	Cfb	Dfb	Dfc	Dfc
Temperature (°C)				
Maximum	27.8	29.4	27.2	25.1
Average	8.8	6.8	1.5	−1.7
Minimum	−12.2	−18.6	−39.0	−41.4
Relative humidity (%)				
Maximum	94	99	99	96
Average	74	79	80	77
Minimum	19	22	18	23
Prevailing direction of WDR	South	Southeast	East	North/South
Average wind velocity (m/s)	2.97	3.13	2.08	3.14
Accumulated rain load (mm/year)	1074	639	502	533
Direction with minimal solar radiation exposure	North	North	North	North

[a]: Cfb: Temperate climate, fully humid, warm summer. Dfb: Snow climate, fully humid, warm summer. Dfc: Snow climate, fully humid, cool summer, and cold winter.

4.2.2 Hygrothermal performance of ACM in the field

The hygrothermal performance of the ACM coating system was evaluated using hygrothermal simulations. Similar to the investigation described in Section 4.2.1, the analyses were conducted for the same four cities in Sweden described in Table 10. The specifications of the simulation model utilized in this evaluation are provided in Table 11. Two distinct scenarios were defined for the long-term analyses based on the orientation of the test wall. In Scenario 1, the orientation was aligned with the prevailing WDR direction, while in Scenario 2, it was set in the direction with minimal drying potential and solar radiation exposure. To enhance the readability, only Scenario 1 is presented in this thesis, while additional information on Scenario 2 is available in **Paper IV**.

Two cases were examined for each scenario, considering AFR values of 0 (no rain) and 0.7 (moderately exposed). In all simulations, a moisture source equivalent to 1% of the WDR on the exterior surface, as defined by ASHRAE Standard 160, was incorporated at the interface between the ACM and brick [36]. This moisture source represented potential water infiltration through cracks or window joints. The transition from a 1D to a 2D model was made to account for the moisture source, representing a one-meter-high test wall. The source was positioned at the vertical midpoint of the wall, with dimensions of 10 mm in width and height. To achieve a dynamic steady-state condition, the simulations were conducted for five consecutive years, utilizing the same one-year weather data from the WUFI. The long-term drying process and the risk of moisture accumulation in the ACM-coated test wall were evaluated by analyzing the total moisture content, W_{tot} (kg/m^3), presented in **Paper IV**. Additionally, the RH levels behind the ACM at position P2 (Figure 16) and the average RH in the ACM layer were assessed. Using the moisture-dependent thermal conductivity of the ACM from (Table 5) and considering the overall RH levels in the ACM, the dynamic thermal conductivity of the ACM in the field was calculated.

Table 11. Scenarios and model specifications used for the long-term hygrothermal analyses on the ACM system.

Exterior heat transfer coefficient	25 (W/[m^2·K])
Interior heat transfer coefficients	8 (W/[m^2·K])
Initial condition (RH)	80% (1st January)
Short-wave radiation absorptivity	0.2
long-wave radiation absorptivity	0.9
Exterior climate	WUFI data file for the considered city
Interior climate	EN 15026
Water-repellent paint (exterior)	sd-value: 0.01
Height of the test wall	1 m
Scenario 1	
Orientation	The prevailing direction of WDR for the considered city (see Table 10.)
AFR	0 and 0.7
Moisture source/Leakage	1% of WDR: at the interface between the ACM and brick
Scenario 2	
Orientation	North: the direction with minimal solar radiation exposure
AFR	0 and 0.7
Moisture source/Leakage	1% of WDR: at the interface between the ACM and brick

4.2.3 Results: hygrothermal simulations

Figure 18 illustrates the estimated duration of the early-stage drying process for the ACM in four Swedish cities at four distinct application times. The findings revealed a range of drying periods, from 134 to 336 days. The longest drying time was observed in Stockholm in September, whereas the shortest was observed in Kiruna in September.

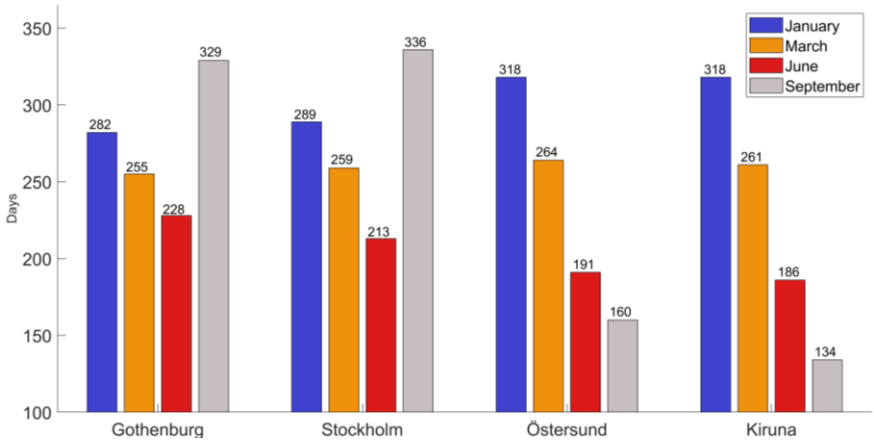

Figure 18. Simulated duration of early-stage drying time in the four Swedish cities at four application times.

The simulated hygrothermal performance of the ACM system in the four studied cities is presented in **Paper IV**, specifically in Figures 11–12 and Appendix B. In the absence of rain (AFR: 0), the RH at the ACM-brick interface (P2) ranged from approximately 20%–60%. However, when rainwater absorption was considered (AFR: 0.7), all cities showed an increase in RH levels at P2, ranging from 29%–81%. These findings demonstrate that regardless of rainwater absorption, the risk of condensation at the ACM-brick interface can be mitigated in all locations, as the RH levels did not exceed 81%. Furthermore, Figure 19 illustrates the moisture-dependent thermal conductivity of the ACM in the four studied cities. The simulations indicate that the thermal conductivities ranged from approximately 42–45 mW/(m·K) without rainwater absorption. However, with rainwater absorption, the thermal conductivity increased by up to 9%, resulting in a range of 42–49 mW/(m·K). Notably, in Gothenburg, where the test wall experienced the highest WDR load, the median thermal conductivity was approximately 3% higher when rainwater absorption was active (AFR: 0.7) than when it was eliminated (AFR: 0).

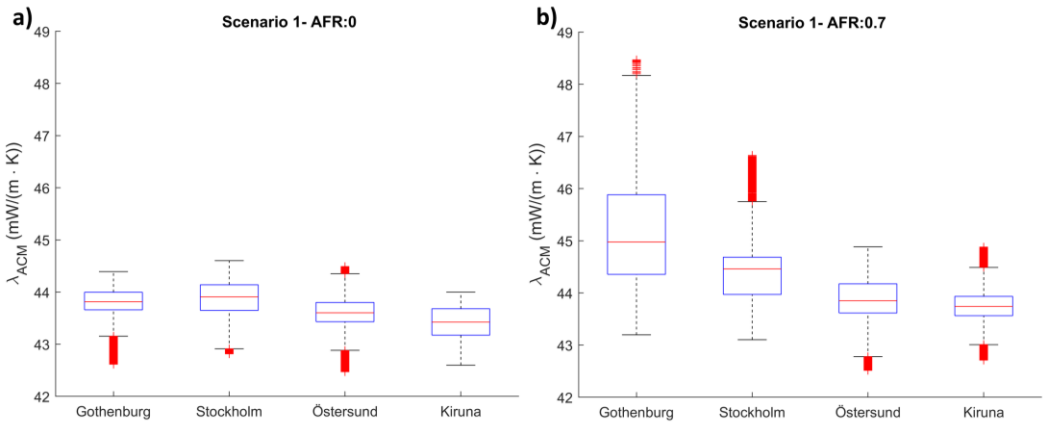

Figure 19. Calculated moisture-dependent thermal conductivity of the ACM. a) AFR:0 (no rain). b) AFR:0.7.

5 General discussions and reflections

This chapter provides general discussions and reflections on the conducted research, highlighting the main contributions of this study to the related research field. The discussions are structured according to the order of the conducted studies, as outlined in Section 1.3.

The research commenced with standardized measurements conducted on the commercial ACM under study, aiming to understand and assess the performance of the fresh mortar and hardened product. During the sample preparation, the specific details of the preparation procedure considerably influenced the final properties of the product. Hence, adherence to the prescribed mixing schedule provided by the producer was crucial to prevent undesired characteristics in the fresh mortar and final product. However, collaborative adjustments with the producer led to improved sample performance. Notably, these challenges and sensitivities were not encountered while preparing similar conventional lime-based coating mortars. Moreover, usually these challenges during ACM sample preparation have not been reported adequately in the literature. This could be due to prior research focusing on in-house-produced trial mixtures, rather than commercial ACMs, designed specifically for research purposes at the laboratory level. Furthermore, the TDS available in 2019 lacks comprehensive and detailed information. However, the present TDS for ACMs offers more comprehensive coverage, encompassing essential details on precise mixing and application processes.

On a positive note, the challenges experienced during the initial stages of the research study served as the underlying motivation for the study presented in **Paper II**. These challenges prompted a thorough assessment of the sample preparations to ensure their alignment with the final commercial product, including measuring and comparing material properties against reported values. Within this process, an unexpected phenomenon of increased water absorptivity of the ACM due to subsequent wetting and drying rounds was observed. Without these initial challenges, the identified phenomenon would possibly have remained unnoticed.

The study presented in **Paper III** introduced the developed runoff setup, which addressed three key criteria that set it apart from existing standard methods used to assess the watertightness of wall assemblies against WDR. As explained in Section 1.3, these three criteria were the capability to work with low-intensity wetting, perform tests on a small scale, and enable precise and real-time monitoring of moisture absorption and distribution during wetting and drying phases. Additionally, a crucial contribution of this research was the incorporation of surface defects (cracks) in assessing the moisture performance of the examined coating system. The low-intensity WDR wetting posed a challenge in the

current development of the setup due to increased complexity and potential measurement uncertainties; therefore, the current study was limited to runoff wetting. Nonetheless, the testing conducted using runoff wetting yielded promising results, describing the effectiveness of the test setup. Moving forward, the next development phase could consider incorporating water spraying and applying overpressure to the test walls.

Regarding the second criterion of small-scale testing, the study demonstrated that downscaled test specimens effectively captured the performance of the tested coating system. However, moisture redistribution occurred vertically due to gravitational forces in test rounds characterized by high water absorption, such as the defective specimens in **Paper III**. The complete sealing of the specimens' sides resulted in moisture accumulation at the lower part of the specimens. This case, attributed to downscaled specimens, may not accurately represent the middle parts of a real-case façade. Instead, it provides an exclusive representation of the bottom parts and corners. However, as sensors were also positioned at the upper parts of the specimens, they could effectively capture the performance representative of the middle part of a large-scale façade. When using large-scale test walls, based on the design of the wetting system, the phenomenon of potential moisture accumulation at the lower parts and its corresponding consequences may not be fully captured or, at the very least, not with the same level of time and practical efficiency, as observed in small-scale test walls.

The monitoring system utilized in the setup consisted of a hanging weighting scale and moisture tracing sensors. The scale demonstrated its capability to accurately capture the mass change of the test specimens, as evidenced by the measurement results. However, as discussed in **Paper III**, the registered mass change by the scale included the weight of the water runoff from the wall surface. Consequently, the reported values for momentaneous water absorption by the test specimen were higher than the actual values. Due to the variability in the amount of water running off the surface, it was challenging to exclude the weight of the water film from the reported values. One potential solution to address this issue in the future could involve installing a second scale to measure the water runoff before it returns to the water supply tank. Despite this limitation, the weighing of the test specimens provided valuable insights into the deviations in the performance of different specimens regarding moisture absorption and drying performance. In the subsequent phase of setup development, addressing the incorporation of overpressure on the test specimen is an important aspect. The oscillation of the suspended specimen resulting from pulsating pressures can potentially disrupt the scale's performance. A potential solution to mitigate the specimen swaying is to attach rods to the setup floor close to the specimen. These rods should be strategically positioned to effectively prevent swaying while ensuring the scale's accuracy remains the same.

To trace the moisture distribution within the ACM system, capacitive moisture sensors were utilized. As discussed in **Paper III** and **Paper IV**, a considerable challenge with many of the commonly used moisture sensors is their time-delayed response to changes in surrounding moisture conditions. The sensors utilized in the field test described in **Paper IV** exhibited response delays ranging from several hours to days upon variations in moisture levels. While these sensors demonstrated stable performance suitable for long-term measurements, alternative sensor types designed for short-term measurements often exhibited reduced durability and were more susceptible to malfunction, particularly in humid environments where corrosion risks existed. However, the tested sensors offered several advantages, including two isolated thin copper electrodes encased in a corrosion-resistant material to prevent contact with water and potential corrosion. The sensors also exhibited rapid and accurate response to changes in moisture levels, as demonstrated in the conducted studies. Furthermore, incorporating an electrical module and compatibility with Internet of Things devices facilitated advanced programming options and enabled real-time data collection and online monitoring during the measurements. This real-time

reading of these sensors and the monitoring scale helped mitigate unforeseen complications and deviations from the intended experimental protocol. During the calibration study, it was observed that the signals obtained from the sensors at moisture levels corresponding to relative humidities of 50%–70% exhibited proximity to each other, whereas this observation was less significant at higher moisture levels. Consequently, to enhance the sampling rate and resolution of future readings, potential improvements could involve implementing an analog-to-digital signal converter with a higher bit length or using an amplifier. In addition, verifying the sensor performance under different climatic conditions and with various material types beyond those considered in this study is advisable.

The field test conducted in **Paper IV** had two primary objectives: first, to gather insights into the application process of the ACM coating system and second, to monitor its drying performance. The test involved measuring two smaller wall partitions within a larger northeast-oriented façade, with each partition covering an approximate area of 3 m^2. Although testing on larger areas would have been preferable, practical, temporal, and financial constraints prohibited such an approach. Testing on a south-oriented façade was unfeasible due to its unavailability. This scenario would have been particularly valuable as it would have exposed the test walls to higher WDR loads. Nonetheless, the northeast-oriented façade provided reduced solar radiation exposure and lower drying potential. Although the interior climate in the tested building was initially intended to be consistently heated throughout the measurement period, practical limitations on site caused sporadic and partial heating. Consequently, the drying process of the ACM coating system was prolonged in its initial stages. Furthermore, the unheated interior prevented the measurement of the thermal insulation properties of the ACM because heat flux measurements were considered less relevant and accurate in this context.

In the numerical simulation study, the WUFI commercial modeling tool was used to investigate the initial drying process and hygrothermal performance of the ACM in four distinct climatic conditions in Sweden. Notably, the climate data files used in the simulations represented typical values from 1995 to 2005 and did not encompass periods with extreme climates. Furthermore, retrofitting moisture-damaged constructions sometimes involves addressing challenges regarding rising dampness and salt efflorescence. However, these specific issues were not considered in the analyses presented in this study. Given rainwater penetration, the ASHRAE Standard 160 [36] recommends considering a water leakage source equivalent to 1% of the rainwater reaching the exterior surface. Similar to previous research on ACMs, such as in [13,37], a moisture source was introduced at the interface between the ACM and the substrate (brick) within the WUFI software. The location of the deposit site can be defined within the meshing domain, which is limited to single or multiple cells. The simplified approach implemented in WUFI assumes that if the moisture content exceeds the water retention capacity of the selected cells, it gradually decreases until full accommodation is achieved. Consequently, any rainwater leakage that cannot be retained by the chosen cells during the specified time is drained away. Thus, the impact of the introduced moisture source is highly dependent on the specified source conditions, geometry, and domain meshing. Several variations in meshing, moisture source conditions, and deposition locations were tested in the analysis. However, these choices induced a minor fluctuation of peak relative humidities, with an increase of less than 4% in the simulations with the highest rain loads in Gothenburg. Nevertheless, this increase in peak relative humidities did not extensively affect the overall conclusions of the study. Considering the substantial computational effort and the requirement for two-dimensional simulations, the inclusion of the moisture source can be disregarded for external ACM systems applied on masonry walls in future works. Alternatively, accurately addressing the effects of rainwater leakage would require a more advanced modeling approach that surpasses the current WUFI methodology.

6 Practical recommendations for the application of ACMs in Sweden

This chapter provides practical recommendations for moisture-safe applications of ACM systems in Sweden.

- The compiled recommendations primarily focus on the external application of ACM systems on concrete and brick masonry walls. Therefore, additional caution must be exercised while considering internal application or applying ACM systems on lightweight structures to ensure adequate drying and moisture safety of the wall assembly. Similarly, when retrofitting existing constructions, especially those with preexisting moisture-related damage, careful attention should be given to ensuring the integrity of the construction. Given material combinations, the studied ACM system presents a moisture-safe design for exterior retrofitting of concrete and masonry, thereby preventing moisture accumulation from rainwater loads. However, additional assessment is required for cases with excessive risk for rising dampness and salt efflorescence, among others. Furthermore, this assessment must consider the interior surface conditions of the wall and the interior climate conditions of the building.

- ACM possesses distinct properties that differ from conventional coating mortars. These properties include lower density, reduced mechanical strength, increased fragility, and higher hydrophobicity. Consequently, ACM is more vulnerable to deviations during the mixing and application phases compared to conventional mortars. Hence, following the instructions outlined in ACM's data sheet is crucial. These instructions provide specific guidelines concerning the mixing procedure and application steps for the fresh mortar (see details in Section 2.1). The protection of the mortar during the application process is equally important, demanding the implementation of weather protection measures and temperature and humidity control. In addition, it is essential to allow the recommended drying and curing time for each layer of the coating system. Usually, an application time of approximately 2 months must be considered. Deviations from these instructions can cause altered material properties, material damage, and eventual performance failure of the final product.

- Careful consideration is necessary for designing and applying the ACM system in high-stress regions, including window details and joints. To maintain the system's mechanical integrity and protect against damage, cracks, and excessive water intrusion through imperfections, the

use of glass-fiber reinforcement mesh is recommended. Consequently, the service life of the ACM system can be extended while minimizing the risk of moisture accumulation.

- When considering the thermal performance and payback period of the ACM, it is essential to account for an initial drying period of approximately 4–12 months before the declared thermal conductivity is achieved. Notably, the thermal conductivity of the ACM may increase by up to 9% due to rainwater absorption. Consequently, water-repellent paint may be recommended for façades that are highly exposed to rain. However, selecting a water-repellent coating for culturally significant structures must sometimes be compatible with the requirements for glare reduction and light reflection.

7 Conclusions

This thesis investigates the moisture absorption of a coating system with aerogel-based coating mortar under three wetting scenarios. It also examines the early-stage drying and long-term hygrothermal performance of the coating system based on the climate conditions in Sweden. Furthermore, the analyses evaluate the influence of surface water-repellent properties and surface cracks on the moisture absorption and drying performance of the coating system. Based on the findings presented in the appended papers **I–IV**, the conclusions of the thesis are summarized below.

At the material level, capillary suction tests were conducted on aerogel-based coating mortar samples to assess their water absorptivity. The results demonstrated a significant increase in capillary water absorptivity with each subsequent wetting and drying round. Notably, the water absorption coefficient after the third round was over five times higher than that of the initial round, with a diminished rate of increase in water absorption between the second and third rounds. This phenomenon suggests potentially unstable material performance over its service life if subjected to free water wetting, potentially introducing uncertainties in moisture risk assessment analyses. However, when the aerogel-based coating mortar was incorporated into the coating system, the capillary suction tests yielded different results. The maximum change in water absorptivity after three rounds of wetting and drying was within 7% compared to that of the first round, indicating a much more stable performance of the coating system compared to the aerogel-based coating mortar used as a standalone material.

At the component level, laboratory testing was conducted to assess the moisture absorption characteristics of the coating system with aerogel-based coating mortar when subjected to runoff wetting. The undamaged coating system exhibited limited moisture absorption, even during prolonged runoff wetting lasting for 24 h. However, when the coating system contained a surface crack of 1 ± 0.5 mm width, the hydrostatic pressure from water runoff increased the water absorption by 2–5 times. This could potentially lead to localized moisture accumulations and a considerable reduction in thermal efficiency by more than 80% compared to the dry state. Furthermore, Karsten tube testing was conducted to simulate water absorption under a high overpressure of up to 1,100 Pa corresponding to a wind velocity of 43 m/s. The results demonstrated that the water absorption during a 90-min wetting period was 2–12 times higher than that of the other wetting scenarios with lower water pressure applied to the surface. As expected, applying water-repellent paint on the coating system's exterior yielded a 50% reduction in water absorption. This has the potential to uphold the thermal insulation properties of the coating system without adversely affecting its drying potential.

The drying of the aerogel-based coating mortar was monitored by field testing conducted in the city of Gothenburg over 15 months. The early-stage drying of the coating material lasted approximately six months, and no sign of moisture accumulation was observed during this initial 15-month period. Considering the climate conditions of Gothenburg, Stockholm, Östersund, and Kiruna, the four Swedish cities under study, numerical hygrothermal simulations were performed to investigate the early-stage drying. Based on the time of application and specific climate conditions, the simulations indicated that the early-stage drying period of the aerogel-based coating mortar ranged from 134 to 336 days. Furthermore, the long-term simulations conducted in these cities revealed no moisture accumulation within the coating system. However, for walls highly exposed to rain, the absorption of rainwater on the exterior surface increased the overall relative humidity within the aerogel-based coating mortar. Consequently, an average increase in thermal conductivity of up to 9% could be expected.

8 Recommendations for future research

Future research should explore the durability and long-term mechanical and hygrothermal performance of ACM-systems. Further investigations are needed to understand the increased capillary water absorption of ACMs during repeated wetting and drying. It is crucial to examine how this phenomenon affects the overall hygrothermal performance of the coating system in-field applications, identify the underlying causes, and determine whether similar phenomena are observed in other ACMs. Consequently, future research could involve studying alternative ACMs available in the European market.

Moreover, further investigation is necessary to explore the economic feasibility of ACMs across various scenarios, including various retrofitting projects and new constructions. In addition, studying the environmental impacts of the production, application, and decommissioning of these mortars is imperative.

The developed small-scale runoff setup is limited to runoff wetting. To expand the research scope, future work should involve upgrades, such as water spraying capabilities and the ability to simulate WDR wetting.

Field testing of the coating system with aerogel-based coating mortar has primarily focused on external applications. Internal applications should further be examined to gain comprehensive insights into its drying performance. Moreover, future research should include extended and diversified field testing that incorporates different weather orientations with higher exposure to WDR. The inclusion of heat flux measurements would enhance understanding of the system's thermal insulation performance in the field. To account for evolving climate conditions, future work should investigate the influence of future climate scenarios on coating system performance.

References

[1] Mjörnell K, Kurkinen E-L. Renovering av befintligt bostadsbestånd 2018. https://www.e2b2.se/library/4084/syntes_e2b2_renovering_av_befintligt_bostadsbestand.pdf (accessed December 2, 2020).

[2] Finansdepartementet- Avdelningen för samhällsplanering och bostäder. PM med Förslag till förordning om stöd till energieffektivisering i flerbostadshus | Enhanced Reader 2021. https://www.regeringen.se/contentassets/daae7190d52e4365bd9298d95dadd311/forslag-till-forordning-om-stod-till-energieffektivisering-i-flerbostadshus.pdf (accessed May 10, 2023).

[3] Boverket. Teknisk status i den svenska bebyggelsen –resultat från projektet BETSI 2011. https://www.boverket.se/globalassets/publikationer/dokument/2011/betst-teknisk-status.pdf (accessed December 2, 2020).

[4] Karim AN, Johansson P, Sasic Kalagasidis A. Knowledge gaps regarding the hygrothermal and long-term performance of aerogel-based coating mortars. Constr Build Mater 2022;314:125602. https://doi.org/10.1016/J.CONBUILDMAT.2021.125602.

[5] Stahl T, Brunner S, Zimmermann M, Ghazi Wakili K. Thermo-hygric properties of a newly developed aerogel based insulation rendering for both exterior and interior applications. Energy Build 2012;44:114–7. https://doi.org/10.1016/J.ENBUILD.2011.09.041.

[6] Karim AN, Johansson P, Kalagasidis AS. Super insulation plasters in renovation of buildings in Sweden: energy efficiency and possibilities with new building materials. IOP Conf Ser Earth Environ Sci 2020;588:042050. https://doi.org/10.1088/1755-1315/588/4/042050.

[7] Fenoglio E, Fantucci S, Perino M, Serra V, Dutto M, Marino V. Energy retrofit of residential buildings with a novel super-insulating aerogel-based plaster. AiCARR J 2020;61:44–8.

[8] Karim AN. Aerogel-based plasters for renovation of buildings in Sweden: Identification of possibilities, information deficiencies and challenges. Licenciate Thesis. Chalmers University of Technology, 2021.

[9] Svensson Tengberg C, Hagentoft C-E. Risk Assessment Framework to Avoid Serial Failure for New Technical Solutions Applied to the Construction of a CLT Structure Resilient to Climate. Buildings 2021;11:247. https://doi.org/10.3390/buildings11060247.

[10] Svensson Tengberg C. A Design-Build Contractor Risk Assessment Framework for New Technical Solutions in the Construction Industry. PhD Thesis. Chalmers University of Technology, 2022.

[11] Kottek M, Grieser J, Beck C, Rudolf B, Rubel F. World map of the Köppen-Geiger climate classification updated. Meteorol Zeitschrift 2006;15:259–63. https://doi.org/10.1127/0941-2948/2006/0130.

[12] Jansson A, Hansén M. Putsade enstegstätade regelväggarErfarenheter från undersökningar som SP har utfört 2015. https://www.diva-portal.org/smash/get/diva2:962875/FULLTEXT01.pdf (accessed December 2, 2020).

[13] Stahl T, Ghazi Wakili K, Hartmeier S, Franov E, Niederberger W, Zimmermann M. Temperature and moisture evolution beneath an aerogel based rendering applied to a historic building. J Build Eng 2017;12:140–6. https://doi.org/10.1016/J.JOBE.2017.05.016.

[14] Ghazi Wakili K, Dworatzyk C, Sanner M, Sengespeick A, Paronen M, Stahl T. Energy efficient retrofit of a prefabricated concrete panel building (Plattenbau) in Berlin by applying an aerogel based rendering to its façades. Energy Build 2018;165:293–300. https://doi.org/10.1016/J.ENBUILD.2018.01.050.

[15] Guizzardi M, Derome D, Vonbank R, Carmeliet J. Hygrothermal behavior of a massive wall with interior insulation during wetting. Build Environ 2015;89:59–71. https://doi.org/10.1016/J.BUILDENV.2015.01.034.

[16] Ganobjak M, Brunner S, Wernery J. Aerogel materials for heritage buildings: Materials, properties and case studies. J Cult Herit 2020;42:81–98. https://doi.org/https://doi.org/10.1016/j.culher.2019.09.007.

[17] Zuo L, Zhang Y, Zhang L, Miao Y-E, Fan W, Liu T. Polymer/Carbon-Based Hybrid Aerogels: Preparation, Properties and Applications. Materials (Basel) 2015;8:6806–48. https://doi.org/10.3390/ma8105343.

[18] Soleimani Dorcheh A, Abbasi MH. Silica aerogel; synthesis, properties and characterization. J Mater Process Technol 2008;199:10–26. https://doi.org/10.1016/j.jmatprotec.2007.10.060.

[19] de Fátima Júlio M, Soares A, Ilharco LM, Flores-Colen I, de Brito J. Aerogel-based renders with lightweight aggregates: Correlation between molecular/pore structure and performance. Constr Build Mater 2016;124:485–95. https://doi.org/10.1016/J.CONBUILDMAT.2016.07.103.

[20] Pedroso M, Flores-Colen I, Silvestre JD, Gomes MG, Silva L, Sequeira P, et al. Characterisation of a multilayer external wall thermal insulation system. Application in a Mediterranean climate. J Build Eng 2020;30:101265. https://doi.org/10.1016/J.JOBE.2020.101265.

[21] Soares A, de Fátima Júlio M, Flores-Colen I, Ilharco LM, Brito J de. EN 998-1 performance requirements for thermal aerogel-based renders. Constr Build Mater 2018;179:453–60. https://doi.org/10.1016/J.CONBUILDMAT.2018.05.197.

[22] Flores-Colen I, Pedroso M, Soares A, Gomes M da G, Ramos NMMR, Maia J, et al. In-Situ Tests on Silica Aerogel-Based Rendering Walls. XV Int. Conf. Durab. Build. Mater. Components, Barcelona: 2020.

[23] Maia J, Pedroso M, Ramos NMM, Pereira PF, Flores-Colen I, Glória Gomes M, et al. Hygrothermal performance of a new thermal aerogel-based render under distinct climatic conditions. Energy Build 2021;243:111001. https://doi.org/10.1016/j.enbuild.2021.111001.

[24] Pedroso M, Flores-Colen I, Silvestre JD, Gomes MG, Silva L, Ilharco L. Physical, mechanical, and microstructural characterisation of an innovative thermal insulating render incorporating silica aerogel. Energy Build 2020;211:109793. https://doi.org/10.1016/J.ENBUILD.2020.109793.

[25] Ibrahim M, Wurtz E, Biwole PH, Achard P, Sallee H. Hygrothermal performance of exterior walls covered with aerogel-based insulating rendering. Energy Build 2014;84:241–51. https://doi.org/10.1016/J.ENBUILD.2014.07.039.

[26] EN 1015-18. Methods of test for mortar for masonry – Part 18: Determination of water absorption coefficient due to capillary action of hardened mortar. 2002.

[27] European Committee for Standardization (CEN). EN 998-1 Specification for mortar for masonry – Part 1: Rendering and plastering mortar. 2016.

[28] Wall systems. HECK AERO iP 2022. https://www.wall-systems.com/produkte/daemmputze-innendaemmung/aero-ip (accessed October 23, 2022).

[29] EN 1015-19. Methods of tests for mortar for masonry – Part 19: Determination of water vapour permeability of hardened rendering and plastering mortars. 1999.

[30] ISO 22007-2. Plastics — Determination of thermal conductivity and thermal diffusivity — Part 2: Transient plane heat source (hot disc) method. 2015.

[31] Draft recommendation for in situ concrete strength determination by combined non-destructive methods. Mater Struct 1993;26:43–9. https://doi.org/10.1007/BF02472237.

[32] LNEC (National Laboratory of Civil Engineering). Wall Coatings. Water Absorption Test under Low Pressure (In Portuguese). Lisbon, Portugal: 2002.

[33] LNEC (National Laboratory of Civil Engineering). In-situ Tests on Wall Coatings for Old Buildings. Preliminary Tests with Karsten Tubes (In Portuguese). Lisbon, Portugal: 2002.

[34] Fraunhofer IBP. WUFI 2020:https://wufi.de/en/. https://wufi.de/en/ (accessed June 15, 2021).

[35] Künzel HM. Simultaneous heat and moisture transport in building components : one- and two-dimensional calculation using simple parameters. PhD thesis. IRB Verlag Stuttgart, 1995.

[36] ASHRAE. Standard 160-2016. Criteria for Moisture-Control Design Analysis in Buildings. ASHRAE Atlanta, GA: 2016.

[37] Pedroso M, Gomes M da G, Silvestre JD, Hawreen A, Flores-Colen I. Thermophysical Parameters and Hygrothermal Simulation of Aerogel-Based Fibre-Enhanced Thermal Insulating Renders Applied on Exterior Walls. Energies 2023, Vol 16, Page 3048 2023;16:3048. https://doi.org/10.3390/EN16073048.